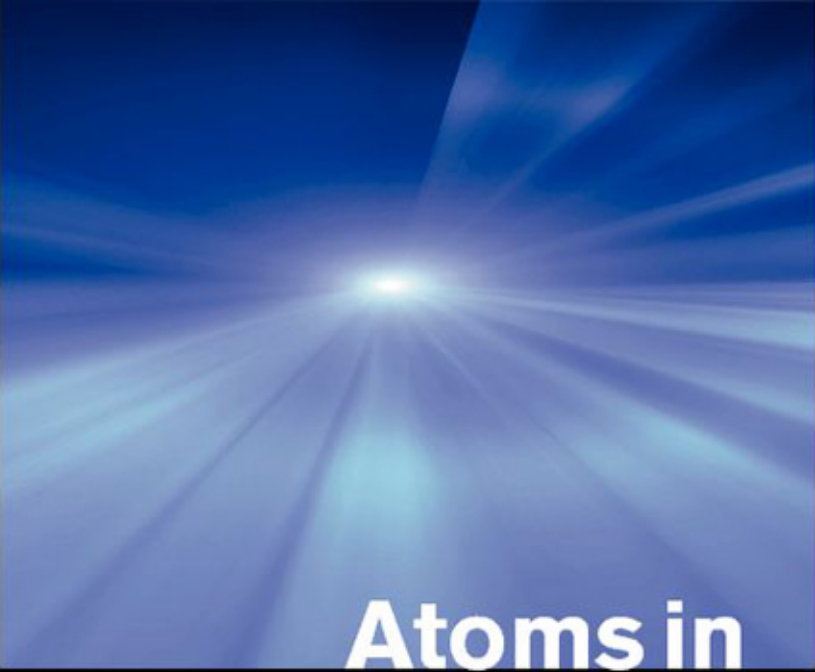

Atoms in Intense Laser Fields

C. J. Joachain
N. J. Kylstra
R. M. Potvliege

CAMBRIDGE

CAMBRIDGE

more information - www.cambridge.org/9780521793018

ATOMS IN INTENSE LASER FIELDS

The development of lasers capable of producing high-intensity pulses has opened a new area in the study of light–matter interactions. The corresponding laser fields are strong enough to compete with the Coulomb forces in controlling the dynamics of atomic systems, and give rise to multiphoton processes. This book presents a unified account of this rapidly developing field of physics.

The first part describes the fundamental phenomena occurring in intense laser–atom interactions and gives the basic theoretical framework to analyze them. The second part contains a detailed discussion of Floquet theory, the numerical integration of the wave equations and approximation methods for the low- and high-frequency regimes. In the third part, the main multiphoton processes are discussed: multiphoton ionization, high harmonic and attosecond pulse generation and laser-assisted electron–atom collisions. Aimed at graduate students in atomic, molecular and optical physics, the book will also interest researchers working on laser interactions with matter.

C. J. JOACHAIN is Emeritus Professor of Theoretical Physics at the University of Brussels. His research activities concern quantum collision theory and the interaction of intense laser fields with matter. He has received many scientific awards and distinctions, in particular the Alexander von Humboldt Prize.

N. J. KYLSTRA is currently employed in the financial services industry, and is a research fellow at the University of Brussels. His research includes the interaction of atoms with high-intensity laser fields.

R. M. POTVLIEGE is currently Reader in Physics at the University of Durham. His research interests cover the theoretical aspects of multiphoton processes in intense laser fields.

ATOMS IN INTENSE LASER FIELDS

C. J. JOACHAIN
University of Brussels

N. J. KYLSTRA
University of Brussels

R. M. POTVLIEGE
University of Durham

CAMBRIDGE
UNIVERSITY PRESS

CAMBRIDGE UNIVERSITY PRESS
Cambridge, New York, Melbourne, Madrid, Cape Town,
Singapore, São Paulo, Delhi, Tokyo, Mexico City

Cambridge University Press
The Edinburgh Building, Cambridge CB2 8RU, UK

Published in the United States of America by Cambridge University Press, New York

www.cambridge.org
Information on this title: www.cambridge.org/9780521793018

First published 2012

Printed in the United Kingdom at the University Press, Cambridge

A catalogue record for this publication is available from the British Library

Library of Congress cataloguing in Publication data
Joachain, C. J. (Charles Jean)
Atoms in intense laser fields / C.J. Joachain, N.J. Kylstra, and R.M. Potvliege.
p. cm.
Includes bibliographical references and index.
ISBN 978-0-521-79301-8 (hardback)
1. Electron-atom collisions. 2. Floquet theory. 3. Laser pulses, Ultrashort. 4. Multiphoton processes.
5. Multiphoton ionization. I. Kylstra, N. J. II. Potvliege, R. M. III. Title.
QC793.5.E628J63 2011
539.7′2–dc23 2011024273

ISBN 978-0-521-79301-8 Hardback

Felix qui potuit rerum cognoscere causas.
(Virgil, Georgics, II, 490)

Contents

Preface *page* xi

Part I Basic concepts 1

1 High-intensity laser–atom physics 3
- 1.1 Introduction 3
- 1.2 High-intensity lasers 5
- 1.3 Multiphoton ionization and above-threshold ionization 10
- 1.4 Harmonic generation and attosecond pulses 21
- 1.5 Laser-assisted electron–atom collisions 29

2 Theory of laser–atom interactions 37
- 2.1 Classical description of a laser field 37
- 2.2 Classical non-relativistic electron dynamics in a laser field 52
- 2.3 Time-dependent Schrödinger equation 57
- 2.4 Gauge transformations 62
- 2.5 The Kramers transformation 65
- 2.6 The evolution operator 66
- 2.7 Gordon–Volkov wave functions 68
- 2.8 Non-dipole effects 71
- 2.9 Relativistic effects 75

Part II Theoretical methods 91

3 Perturbation theory 93
- 3.1 Time-dependent perturbation theory for the evolution operator 93
- 3.2 Method of variation of the constants 125
- 3.3 Semi-perturbative methods 137

4 Floquet theory 141
4.1 Hermitian Floquet theory 142
4.2 Bound–bound Floquet dynamics 155
4.3 Floquet dressed continuum states 170
4.4 Non-Hermitian Floquet theory 179
4.5 Floquet theory in the Kramers–Henneberger frame 191
4.6 Sturmian-Floquet theory 194
4.7 R-matrix–Floquet theory 196

5 Numerical integration of the wave equations 218
5.1 Discrete-time propagators, representations of the wave function and choice of gauge 219
5.2 Calculation of the observables 232
5.3 One- and two-dimensional studies of the time-dependent Schrödinger equation 236
5.4 Time-dependent Schrödinger equation for atomic hydrogen 241
5.5 Time-dependent Schrödinger equation for complex atoms 247
5.6 Non-dipole effects 258
5.7 Relativistic effects 260

6 The low-frequency regime 267
6.1 Quasi-static ionization 268
6.2 Multiphoton processes in the strong-field approximation 281
6.3 Multiphoton direct ionization 288
6.4 High harmonic generation 305
6.5 Recollision ionization 320
6.6 Non-dipole effects 323

7 The high-frequency regime 334
7.1 High-frequency Floquet theory 334
7.2 Structure of atomic hydrogen in intense, high-frequency laser fields 340
7.3 Atomic stabilization 350

Part III Multiphoton atomic physics 375

8 Multiphoton ionization 377
8.1 Multiphoton single ionization 377
8.2 Multiphoton double ionization 398

9 Harmonic generation and attosecond pulses 418
9.1 Experiments 418

9.2 Calculations 422
9.3 Properties of harmonics and applications 439
9.4 Attosecond pulses 444

10 Laser-assisted electron–atom collisions 466
10.1 Experiments 468
10.2 Laser-assisted potential scattering 472
10.3 Laser-assisted collisions of electrons with real atoms 500

Appendix: Atomic units and conversion factors 550

Author index 552

Subject index 564

Preface

The availability of intense laser fields over a wide frequency range, in the form of short pulses of coherent radiation, has opened a new domain in the study of light–matter interactions. The peak intensities of these laser pulses are so high that the corresponding laser fields can compete with the Coulomb forces in controlling the dynamics of atomic systems. Atoms interacting with such intense laser fields are therefore exposed to extreme conditions, and new phenomena occur which are known as multiphoton processes. These phenomena generate in turn new behaviors of bulk matter in strong laser fields, with wide-ranging applications.

The purpose of this book is to give a self-contained and unified presentation of high- intensity laser–atom physics. It is primarily aimed at physicists studying the interaction of laser light with matter at the microscopic level, although it is hoped that any scientist interested in laser–matter interactions will find it useful.

The book is divided into three parts. The first one contains two chapters, in which the basic concepts are presented. In Chapter 1, we give a general overview of the new phenomena discovered by studying atomic multiphoton processes in intense laser fields. In Chapter 2, the theory of laser–atom interactions is expounded, using a semi-classical approach in which the laser field is treated classically, while the atom is described quantum mechanically. The wave equations required to study the dynamics of atoms interacting with laser fields are discussed, starting with the non-relativistic time-dependent Schrödinger equation in the dipole approximation, then moving to the description of non-dipole effects and finally to relativistic wave equations.

The second part, containing five chapters, is devoted to a detailed discussion of the most important theoretical methods used to solve the wave equations given in Chapter 2. We begin, in Chapter 3, by considering perturbation theory, which can only be employed for laser fields having moderate intensities and for non-resonant multiphoton processes. In the next four chapters we discuss non-perturbative methods, which must be used when atoms interact with strong laser

fields. In Chapter 4, we review the Floquet theory, in particular the Sturmian-Floquet and R-matrix–Floquet methods. Chapter 5 is devoted to the numerical solution of the wave equations. Approximation methods appropriate to investigate the interaction of atoms with low-frequency and high-frequency laser fields are considered in Chapters 6 and 7, respectively. It is remarkable that in these two distinct frequency regimes, simple theoretical considerations provide considerable insight into the physics of intense laser–atom interactions.

In the third part of the book, which contains the final three chapters, the methods discussed in the second part are applied to the analysis of the three most important atomic multiphoton processes in intense laser fields: multiphoton ionization, harmonic generation and laser-assisted electron–atom collisions. Thus, in Chapter 8 we discuss successively multiphoton single and double ionization of atoms. In Chapter 9, after analyzing the emission of harmonics by atoms, we review the generation and characterization of attosecond pulses, and their use in the new field of attophysics. Finally, in Chapter 10, we begin our theoretical analysis of laser-assisted electron–atom collisions by considering the simple case for which the target atom is modeled by a potential. We then turn our attention to collisions with real atoms having an internal structure.

We wish to thank our colleagues and students for numerous helpful discussions and suggestions. One of us (C.J.J.) would like to acknowledge the hospitality of the Max-Planck Institut für Quantenoptik in Garching, where he was the guest of Professor H. Walther and more recently of Professor F. Krausz. We would also like to thank Professor H. Joachain-Bukowinski and Professor N. Vaeck for their help in preparing the diagrams.

Part I

Basic concepts

1

High-intensity laser–atom physics

In recent years, intense laser fields have become available, over a wide frequency range, in the form of short pulses. Such laser fields are strong enough to compete with the Coulomb forces in controlling the dynamics of atomic systems. As a result, atoms in intense laser fields exhibit new properties that have been discovered via the study of *multiphoton processes*. After some introductory remarks in Section 1.1, we discuss in Section 1.2 how intense laser fields can be obtained by using the "chirped pulse amplification" method. In the remaining sections of this chapter, we give a survey of the new phenomena discovered by studying three important multiphoton processes in atoms: multiphoton ionization, harmonic generation and laser-assisted electron–atom collisions.

1.1 Introduction

If radiation fields of sufficient intensity interact with atoms, processes of higher order than the single-photon absorption or emission play a significant role. These higher-order processes, called multiphoton processes, correspond to the net absorption or emission of more than one photon in an atomic transition. It is interesting to note that, in the first paper he published in *Annalen der Physik* in the year 1905, his "Annus mirabilis," Einstein [1] not only introduced the concept of "energy quantum of light" – named "photon" by Lewis [2] in 1926 – but also mentioned the possibility of multiphoton processes occurring when the intensity of the radiation is high enough, namely "if the number of energy quanta per unit volume simultaneously being transformed is so large that an energy quantum of emitted light can obtain its energy from several incident energy quanta." Multiphoton processes were also considered in the pioneering work of Göppert-Mayer [3].

There are several types of multiphoton processes. For instance, an atom can undergo a transition from a bound state to another bound state of higher energy via the absorption of n photons ($n \geq 2$), a process known as *multiphoton excitation*.

Also, an atom in an excited state can emit n photons in a transition to a state of lower energy, a process called *multiphoton de-excitation*, either by spontaneous emission (which does not require the presence of an external radiation field) or by stimulated emission. Another example is the *multiphoton ionization* (MPI) of an atom, a process in which the atom absorbs n photons, and one or several of its electrons are ejected. An atom interacting with a strong laser field can also emit radiation at higher-order multiples, or harmonics, of the frequency of the laser; this process is known as *harmonic generation*. Finally, radiative collisions involving the exchange (absorption or emission) of n photons can occur in *laser-assisted atomic collisions* such as electron–atom or atom–atom collisions in the presence of a laser field.

Except for spontaneous emission, which will not be considered here, the observation of multiphoton transitions requires relatively large laser intensities. Typically, intensities of the order of $10^8\,\mathrm{W\,cm^{-2}}$ are required to observe multiphoton transitions in laser-assisted electron–atom collisions, while intensities of $10^{10}\,\mathrm{W\,cm^{-2}}$ are the minimum necessary for the observation of multiphoton ionization in atoms. In fact, such intensities are now considered to be rather modest. Indeed, as we shall see in the following section, laser fields have become available in the form of short pulses having intensities of the order of, or exceeding, the atomic unit of intensity

$$I_\mathrm{a} = \frac{1}{2}\epsilon_0 c \mathcal{E}_\mathrm{a}^2 \simeq 3.5 \times 10^{16}\,\mathrm{W\,cm^{-2}}, \tag{1.1}$$

where c is the velocity of light in vacuo, ϵ_0 is the permittivity of free space and $\mathcal{E}_\mathrm{a}$ is the atomic unit of electric field strength, namely

$$\mathcal{E}_\mathrm{a} = \frac{e}{(4\pi\epsilon_0)a_0^2} \simeq 5.1 \times 10^9\,\mathrm{V\,cm^{-1}}, \tag{1.2}$$

where e is the absolute value of the electron charge and a_0 is the first Bohr radius of atomic hydrogen. Atomic units (a.u.) are discussed in the Appendix. We note that $\mathcal{E}_\mathrm{a}$ is the strength of the Coulomb field experienced by an electron in the first Bohr orbit of the hydrogen atom. Laser fields having intensities of the order of, or larger than, I_a are strong enough to compete with the Coulomb forces in governing the dynamics of atoms. Thus, while multiphoton processes involving laser fields with intensities $I \ll I_\mathrm{a}$ can be studied by using perturbation theory, the effects of laser fields with intensities of the order of, or exceeding, I_a must be analyzed by using non-perturbative approaches.

In Chapter 2, we shall discuss the theory of laser–atom interactions based on a semi-classical approach which provides the framework for studying atomic multiphoton processes in intense laser fields. In particular, we shall introduce the *dipole approximation*, in which the laser field is described by a spatially homogeneous electric-field component, while its magnetic-field component vanishes. The dipole approximation is fully adequate to investigate atomic multiphoton processes over a

wide range of laser frequencies and intensities. However, as the intensity increases beyond critical values that depend on the frequency, *non-dipole* effects due to the magnetic-field component of the laser field, and eventually *relativistic* effects, must be taken into account [4–7].

The theoretical methods required to solve the quantum-mechanical wave equations introduced in Chapter 2 will be developed in the second part of this book (Chapters 3–7). We shall discuss powerful *ab initio* methods such as the Sturmian-Floquet method [8, 9], the R-matrix–Floquet method [10, 11] and the numerical solution of the time-dependent Schrödinger equation [12, 13]. In this second part, we shall also examine *methods of approximation* which can be used to analyze multiphoton processes at low or at high laser frequencies, respectively. All of these methods will be applied in the third part (Chapters 8–10) to analyze atomic multiphoton processes.

The subject of atoms in intense laser fields has been covered in the volumes edited by Gavrila [14] and by Brabec [15], in the review articles by Burnett, Reed and Knight [16], Joachain [17], Kulander and Lewenstein [18], Protopapas, Keitel and Knight [19], Joachain, Dörr and Kylstra [20], Milosevic and Ehloztky [21], and also in the books by Faisal [22], Mittleman [23], Delone and Krainov [24] and Grossmann [25].

1.2 High-intensity lasers

To obtain high-intensity laser fields, one must concentrate large amounts of energy into short periods of time, and then focus the laser light onto small areas. In an intense laser system, the oscillator produces a train of pulses of short duration. The amplifier then increases the energy of the pulses, which are subsequently focused. A very successful method of amplification, called "chirped pulse amplification" (CPA), was devised in 1985 by Strickland and Mourou [26]. This method, which is illustrated in Fig. 1.1, consists in the following three steps. Firstly, the short laser pulse to be amplified (produced by the oscillator) is stretched in time into its frequency components by a dispersive system such as a pair of diffraction gratings, so that a *chirped* pulse is generated. This stretching in time of the pulse greatly reduces its peak intensity, so that in the second step the frequency components of the chirped pulse can be sent in succession through a laser amplifier without distortions and damage. In the third step, the amplified chirped pulse is compressed in time by another pair of diffraction gratings, which recombine the dispersed frequencies, thus producing a short pulse with a very large peak intensity. Finally, the resulting amplified short pulse is tightly focused onto a small area. After focusing, intensities of the order of the atomic unit of intensity I_{a} can be readily obtained. An important advantage of the CPA method is that it can yield very intense, short pulses by using

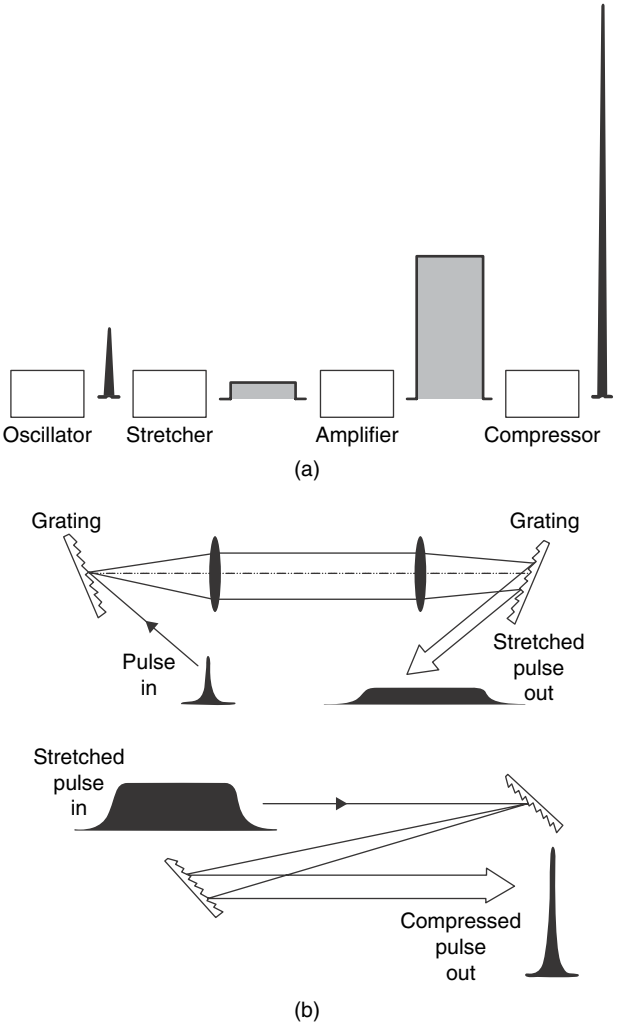

Figure 1.1. Chirped pulse amplification (CPA) method. (a) An oscillator produces a short pulse, which is then chirped (stretched in time into its frequency components). In this way, the peak intensity of the pulse is lowered, so that amplification can take place without damage or distortions. The amplified chirped pulse is then compressed in time, resulting in a short pulse with a very high intensity. (b) The matched stretcher and compressor of the CPA method. The stretcher (top) consists of a telescope of magnification unity placed between two antiparallel gratings. In this configuration, the low-frequency components of the pulse have a shorter optical path than the high-frequency ones. Conversely, the compressor (bottom) consists of a pair of parallel gratings, so that the optical path for the high-frequency components of the pulse is shorter than for the low-frequency ones. (From G. A. Mourou, C. P. J. Barty and M. D. Perry, *Phys. Today*, **Jan**., 22 (1998).)

a "table-top" laser system. A review of the CPA method has been given by Mourou, Tajima and Bulanov [27].

The first CPA high-intensity lasers to be constructed used Nd:glass as the amplifying medium. In the system developed during the 1990s at Imperial College, London, a pulse from a Nd oscillator, of wavelength $\lambda = 1064\,\text{nm}$, duration 1 ps ($10^{-12}$ s) and energy 1 nJ was stretched by diffraction gratings to about 25 ps. It was then amplified by using Nd:glass as the amplifying medium to an energy of about 1 J. This amplified chirped pulse was subsequently compressed to a duration close to its initial picosecond value by diffraction gratings, so that output powers of around 1 TW (10^{12} W) could be obtained. By focusing over an area having a diameter of 10 μm, intensities of the order of $10^{18}\,\text{W cm}^{-2}$ were reached. Lasers of this kind have a repetition rate of about one shot per minute. More recently, CPA laser systems employing Ti:sapphire for the oscillator and the amplifying medium have been used extensively, because they can generate very short pulses with high repetition rates. If only moderate intensities ($\sim 10^{14}\,\text{W cm}^{-2}$) are required, such laser systems can produce pulses having a duration of about 30 fs, with a repetition rate of 300 kHz. CPA Ti:sapphire lasers can also yield very intense pulses. For example, at the ATLAS laser facility in the Max-Planck Institut für Quantenoptik in Garching, pulses of 100 fs in duration and 1 nJ in energy have been stretched, amplified and compressed, giving output pulses of wavelength $\lambda = 790\,\text{nm}$, duration 150 fs and energy 220 mJ at a repetition rate of 10 Hz. After focusing on a spot 6 μm in diameter, the intensity available from this laser reached $4 \times 10^{18}\,\text{W cm}^{-2}$. More recently, intensities up to $10^{22}\,\text{W cm}^{-2}$ have been achieved using the Hercules Ti:sapphire laser at the University of Michigan [28].

The CPA concept was originally developed for the amplification of short laser pulses with laser amplifiers based on laser gain media. However, it was subsequently realized that it can also be used with optical parametric amplifiers (OPA), in which case it is known as the *optical parametric chirped pulse amplification* (OPCPA) method [29, 30]. Optical parametric amplification [31, 32] is a second-order phenomenon of non-linear optics, arising from the fact that crystal materials lacking inversion symmetry can display a $\chi^{(2)}$ non-linearity, where $\chi^{(n)}$ denotes the nth-order susceptibility [33]. Apart from other effects (frequency doubling, generation of sum and difference frequencies), this gives rise to parametric amplification, in which a weak signal beam of angular frequency ω_1 and an intense pump beam of angular frequency $\omega_3 > \omega_1$ generate two intense beams with angular frequencies ω_1 and $\omega_2 = \omega_3 - \omega_1$. Indeed, as the signal beam and the pump beam propagate together through the crystal, photons of the pump beam, having energy $\hbar\omega_3$, are converted into lower-energy signal photons of energy $\hbar\omega_1$ and an equal number of "idler" photons of energy $\hbar\omega_2 = \hbar(\omega_3 - \omega_1)$, where $\hbar = h/(2\pi)$ and h is Planck's constant. A schematic diagram of an optical parametric amplifier is shown in Fig. 1.2.

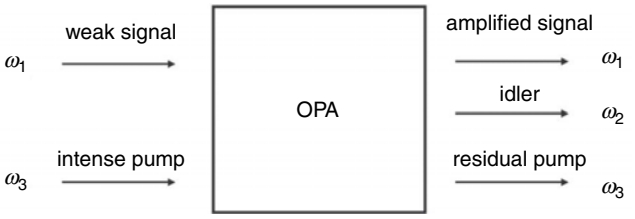

Figure 1.2. Optical parametric amplifier.

Recent technological advances in ultra-fast optics have allowed the generation of intense laser pulses comprising only a few optical cycles (that is, laser periods, where the laser period is defined as $T = 2\pi/\omega$) of the laser field [34, 35]. In particular, the development of Ti:sapphire laser systems using the CPA method has made possible the generation of such high-intensity "few-cycle pulses" in the near infra-red region of the electromagnetic spectrum, with a central wavelength around 800 nm, corresponding to a photon energy of 1.55 eV and an optical cycle of 2.7 fs.

A successful way of obtaining intense few-cycle laser pulses relies on external bandwidth broadening of amplified pulses in gas-filled capillaries [36, 37], using the hollow-fiber technique [38] and chirped-mirror technology [39]. For example, using a Ti:sapphire laser system and a hollow-fiber chirped-mirror compressor, Sartania *et al.* [37] demonstrated the generation of 0.1 TW, 5 fs laser pulses at a repetition rate of 1 kHz. However, the method of gas-filled capillaries involves important energy losses and is difficult to scale to very high energies and peak powers. Several OPCPA systems delivering very intense, few-cycle 800 nm laser pulses have also been reported [40–43].

In addition to very high peak intensities and high repetition rates, the laser systems delivering few-cycle pulses must also provide reliable control over the *carrier-envelope phase* (CEP) φ, namely the phase of the carrier wave with respect to the maximum of the laser pulse envelope, since the CEP sensitively determines the variation of the electric field [44].

As an example, we show in Fig. 1.3 the wave form of the electric field of a linearly polarized laser pulse whose carrier wavelength is $\lambda = 800$ nm and whose intensity profile is proportional to $F(t)\cos(\omega t + \varphi)$, where $F(t)$ is a sech envelope function. In Fig. 1.3(a), the CEP is $\varphi = 0$, corresponding to a "cosine-like" pulse, while in Fig. 1.3(b) the CEP is $\varphi = -\pi/2$, corresponding to a "sine-like" pulse.

Intense few-cycle laser pulses with stabilized CEP have been obtained by using CPA Ti:sapphire laser systems [45–56]. A few-cycle OPCPA system producing infra-red laser pulses at a wavelength of 2.1 μm with a stable CEP has also been demonstrated [57]. One of the major goals is to perform a *single-shot* determination

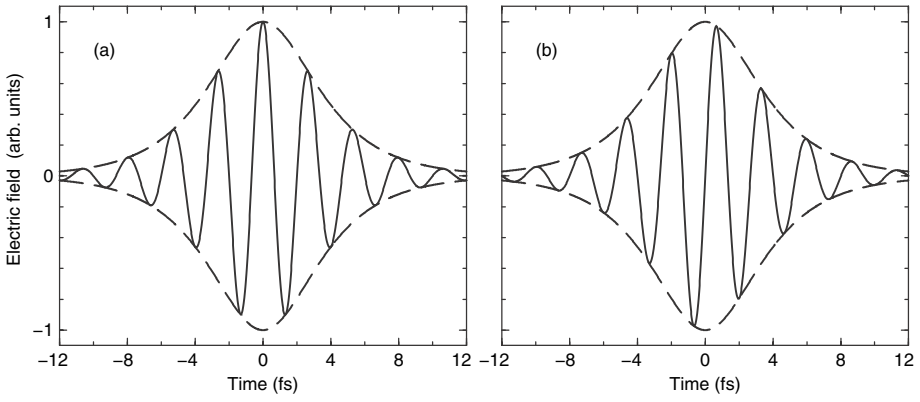

Figure 1.3. Wave form of the electric field (solid curves) of a linearly polarized laser pulse, taken to be proportional to $F(t)\cos(\omega t + \varphi)$, where $F(t)$ is a sech envelope function such that $F^2(t)$ is a sech^2 function of 5 fs full width at half maximum (dashed curves). The carrier wavelength is $\lambda = 800$ nm and the carrier-envelope phase is (a) $\varphi = 0$ for the "cosine-like" pulse and (b) $\varphi = -\pi/2$ for the "sine-like" pulse.

of the CEP of the laser system, while using only a relatively small fraction of the available laser pulse energy.

Intense few-cycle laser pulses with a stable CEP play an important role in high-intensity laser–matter interactions. Indeed, with such pulses, complete control of the electric field wave form of the laser pulse is obtained, since the pulse shape, the carrier wavelength and the carrier-envelope phase can all be determined. As a result, these pulses provide a new way to study the electron dynamics in intense laser–atom processes. They can exert a controlled force on electrons that may vary on atomic scales, not only in strength, but also in time.

Most of the work in the area of high-intensity laser–matter interactions has been restricted to infra-red, visible and ultra-violet radiation [58,59]. With the advent of *free electron lasers*, another source has become available to perform experiments over a wide range of wavelengths extending from the millimeter to the X-ray domains [60].

In a free-electron laser (FEL), an electron beam moving at a relativistic velocity passes through a periodic, transverse magnetic field produced by arranging magnets with alternating poles along the beam path. This array of magnets is called an undulator or wiggler because it forces the electrons to acquire a wiggle motion in the plane orthogonal to the magnetic field. This transverse acceleration produces spontaneous longitudinal emission of electromagnetic radiation of the synchrotron radiation type. Laser action is due to the fact that the electron motion is in phase with the electromagnetic field of the radiation already emitted, so that the fields

add coherently and further emission is stimulated. Free-electron lasers have many attractive properties such as wide tunability and high laser power. However, they are large and expensive, since they involve using electron beam accelerators. The first FEL was demonstrated at a wavelength of 3.4 μm using the Stanford Linear Accelerator [61]. Since then, several FELs have been operated at wavelengths ranging from the millimeter to the soft X-ray region.

In the short-wavelength (VUV and X-ray) region, the lack of appropriate mirrors prevents the operation of an FEL oscillator. As a result, there must be suitable amplification during a single pass of the electron beam through the undulator. It is worth noting that even if the initial electromagnetic field is zero, laser action can still occur in the FEL through the process of "self-amplified spontaneous emission" (SASE), whereby shot noise in the electron beam causes a noisy signal to be initially radiated. This noise then acts as a seed for the FEL, so that the amplification process develops and intense coherent radiation is produced in a narrow band around the resonance wavelength. The first observation of the SASE process was reported at the Free Electron Laser in Hamburg (FLASH) at a wavelength of 109 nm [62]. Also at the FLASH facility, short VUV laser pulses of wavelengths in the range 95–105 nm, durations of 30–100 fs and peak powers at the gigawatt level have been generated [63]. More recently, lasing was observed by the FLASH team at a wavelength of 6.5 nm, in the soft X-ray domain. The European X-ray Free Electron Laser (XFEL) in Hamburg and the Linac Coherent Light Source (LCLS) at Stanford, both under development, will operate at wavelengths down to around 0.1 nm, well into the X-ray region.

1.3 Multiphoton ionization and above-threshold ionization

In this section, we give a survey of the basic features of the *multiphoton ionization* (MPI) process, starting with the multiphoton *single* ionization reaction

$$n\hbar\omega + A^q \rightarrow A^{q+1} + \mathrm{e}^- , \tag{1.3}$$

where q is the charge of the target atomic system A, expressed in atomic units, $\hbar\omega$ is the photon energy and n is a positive integer.

This process was first observed in 1963 by Damon and Tomlinson [64], who used a ruby laser to ionize helium, argon and a neutral air mixture. In subsequent investigations, Voronov and Delone [65] used a ruby laser to induce seven-photon ionization of xenon, and Hall, Robinson and Branscomb [66] recorded two-photon electron detachment from the negative ion I^-. In later years, important results were obtained by several experimental groups, in particular at Saclay, where the dependence of the ionization rates on the laser intensity were studied. For the intensities $I \ll I_\mathrm{a}$ available at that time, it was observed that the total n-photon

ionization rate was proportional to I^n. As we shall see in Chapter 3, this result is in agreement with the prediction of the lowest (non-vanishing) order of perturbation theory (LOPT). At that time, the phenomenon of resonantly enhanced multiphoton ionization (REMPI) was also studied.

A crucial breakthrough was made when experiments detecting the energy-resolved photoelectrons were performed. In this way, Agostini *et al.* [67] discovered in 1979 that at sufficiently high intensities ($I > 10^{11}\,\mathrm{W\,cm^{-2}}$), the ejected electron can absorb photons in excess of the minimum number required for ionization to occur. This phenomenon is called "above-threshold ionization" (ATI). The photoelectron spectra were seen to consist of several peaks, separated by the photon energy $\hbar\omega$, and appearing at energies E_s satisfying the generalized Einstein equation

$$E_s = (n_0 + s)\hbar\omega - I_\mathrm{P}\,, \tag{1.4}$$

where n_0 is the minimum number of photons needed to exceed the field-free ionization potential I_P of the atom and $s = 0, 1, \ldots$ is the number of excess photons (or "above-threshold" photons) absorbed by the atom.

A typical example of ATI photoelectron energy spectra, measured in 1988 by Petite, Agostini and Muller [68], is shown in Fig. 1.4. Pulses of 130 ps duration obtained from a Nd:YAG laser of wavelength $\lambda = 1064\,\mathrm{nm}$ were focused into a xenon vapor, and the electron energy spectrum was recorded using a time of flight spectrometer, with a 25 meV resolution. At relatively weak intensities, the

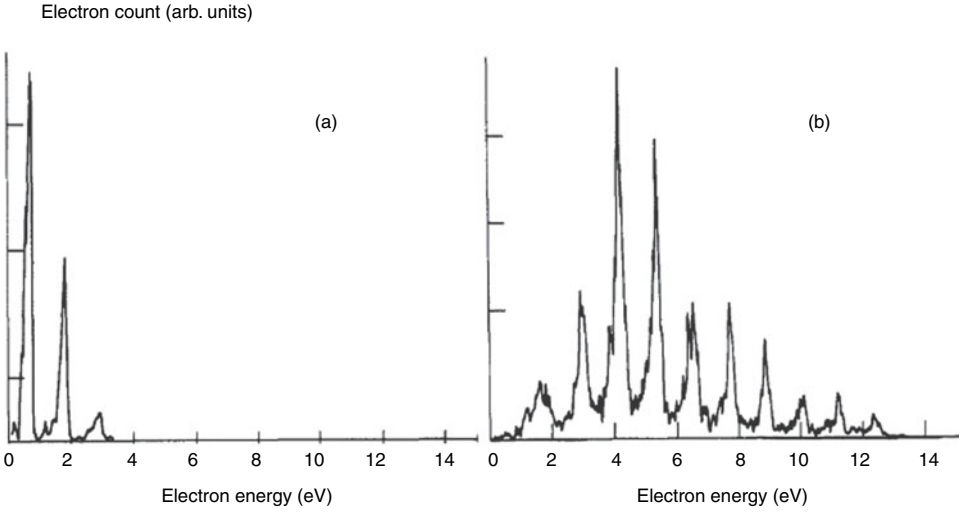

Figure 1.4. Electron energy spectra showing "above-threshold ionization" (ATI) of xenon at a laser wavelength $\lambda = 1064\,\mathrm{nm}$. (a) $I = 2.2 \times 10^{12}\,\mathrm{W\,cm^{-2}}$, (b) $I = 1.1 \times 10^{13}\,\mathrm{W\,cm^{-2}}$. (From G. Petite, P. Agostini and H. G. Muller, *J. Phys. B* **21**, 4097 (1988).)

intensity dependence of the peaks follows the LOPT prediction according to which the ionization rate for an (n_0+s)-photon process is proportional to I^{n_0+s} (see Fig. 1.4(a)). As the intensity increases, peaks at higher energies appear (see Fig. 1.4(b)), whose intensity dependence does not follow the I^{n_0+s} prediction of LOPT.

Another remarkable feature of the ATI spectrum in Fig. 1.4(b) is that as the intensity increases, the low-energy peaks are reduced in magnitude. The reason for this *peak suppression* is that the energies of the atomic states are *Stark-shifted* in the presence of a laser field. For low laser frequencies (for example, a Nd:YAG laser with photon energy $\hbar\omega = 1.17\,\text{eV}$), the AC Stark shifts of the lowest bound states are small in magnitude. On the other hand, the induced Stark shifts of the Rydberg and continuum states are essentially given by the electron *ponderomotive energy* U_p, which is the cycle-averaged kinetic energy of a quivering electron in a laser field. For a monochromatic laser field, it is given by

$$U_\text{p} = \frac{e^2\mathcal{E}_0^2}{4m\omega^2}\,, \tag{1.5}$$

where m is the mass of the electron and $\mathcal{E}_0$ is the electric field strength. It is worth noting that the ponderomotive energy U_p is proportional to I/ω^2, and may become quite large. For example, in the case of a Nd:YAG laser of wavelength $\lambda = 1064\,\text{nm}$, the ponderomotive energy U_p given by Equation (1.5) becomes equal to the laser photon energy $\hbar\omega = 1.17\,\text{eV}$ at an intensity $I \simeq 10^{13}\,\text{W cm}^{-2}$. Since the energies of the Rydberg and continuum states are shifted upwards relative to the lower bound states by about U_p, there is a corresponding increase in the intensity-dependent ionization potential $I_\text{P}(I)$ of the atom, so that $I_\text{P}(I) \simeq I_\text{P} + U_\text{p}$. If this increase is such that $n\hbar\omega < I_\text{P} + U_\text{p}$, then ionization by n photons is energetically forbidden (see Fig. 1.5). However, atoms interacting with smoothly varying pulses experience a range of intensities, so that the corresponding peak in the photoelectron spectrum will not completely disappear, as seen in Fig. 1.4(b).

For relatively long pulses (in the picosecond range), the photoelectron escapes from the focal volume while the laser field is still present, so that it experiences a force due to the spatial inhomogeneity of the laser field intensity. The electron quiver motion is then converted into radial motion out of the laser focal region, increasing its kinetic energy by U_p, and hence exactly canceling the decrease in energy caused by the (Stark-shifted) increase in the ionization potential. As a result, the photoelectron energies are given by Equation (1.4). However, as noted above, the first ATI peak will nearly disappear if U_p exceeds the photon energy $\hbar\omega$. Similarly, the first two peaks will be weakened if U_p exceeds $2\hbar\omega$, etc. It should be noted that in this long-pulse limit, the photoelectrons have a kinetic energy at least equal to U_p once they have left the laser beam.

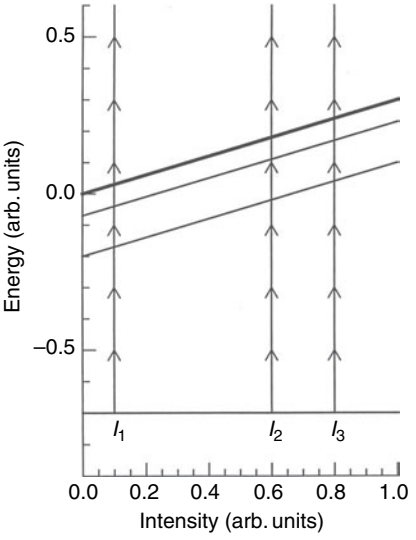

Figure 1.5. Mechanism responsible for the suppression of low-energy peaks in ATI spectra. For low laser frequencies, the intensity-dependent ionization potential of the atom, $I_P(I)$, is such that $I_P(I) \simeq I_P + U_p$, and hence increases linearly with the intensity I. Ionization by four photons, which is possible at the intensity I_1, for which $4\hbar\omega \geq I_P + U_p$, is prohibited at the higher intensities I_2 and I_3, where five photons are needed to ionize the atom. Also illustrated is the mechanism responsible for the resonantly induced structures appearing in ATI spectra for short laser pulses. At the intensity I_2, a Rydberg state has shifted into four-photon resonance with the ground state.

For short (sub-picosecond) laser pulses, the laser field turns off before the photoelectron can escape from the focal volume. In this case, the quiver energy is returned to the laser field and the ATI spectrum becomes more complicated. The observed photoelectron energies are given by the values

$$\tilde{E}_s = (n_0 + s)\hbar\omega - (I_P + U_p) \tag{1.6}$$

relative to the *shifted* ionization potential $I_P + U_p$. Photoelectrons originating from different regions of the focal volume are thus emitted with different ponderomotive shifts. As a result, the ATI peaks exhibit a substructure which, as seen from Fig. 1.5, arises from the fact that the intensity-dependent Stark shifts bring different states of the atom into multiphoton resonance during the laser pulse. An example of such substructure due to the REMPI phenomenon, observed by Freeman *et al.* [69], is shown in Fig. 1.6. This substructure is not seen in long-pulse experiments because in that case, as explained above, the photoelectrons regain their ponderomotive energy deficit from the laser field as they escape from the focal volume.

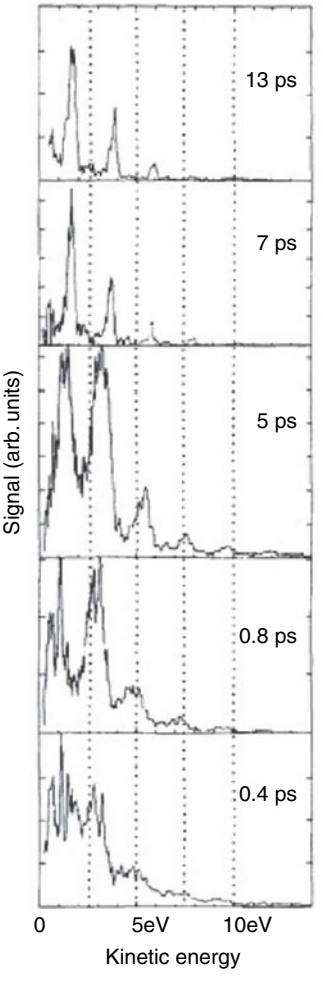

Figure 1.6. Kinetic energy of photoelectrons emitted from xenon as a function of the laser pulse width. The pulse energy is held roughly constant for all runs, so that the intensity increases from about $1.2 \times 10^{13}\,\mathrm{W\,cm^{-2}}$ for 13 ps to about $3.9 \times 10^{14}\,\mathrm{W\,cm^{-2}}$ for 0.4 ps. For the shortest-pulse widths, the individual ATI peaks break up into a narrow fine structure. (From R. R. Freeman *et al.*, *Phys. Rev. Lett.* **59**, 1092 (1987).)

If the frequency is low enough and the laser field is sufficiently strong, ionization can be interpreted by using a quasi-static model in which the bound electrons experience an effective potential formed by adding to the atomic potential the contribution due to the instantaneous laser electric field (see Fig. 1.7(a)). The "instantaneous" ionization rate may then be approximated by the static-limit tunneling rate which can be calculated for hydrogenic systems using the formula given by

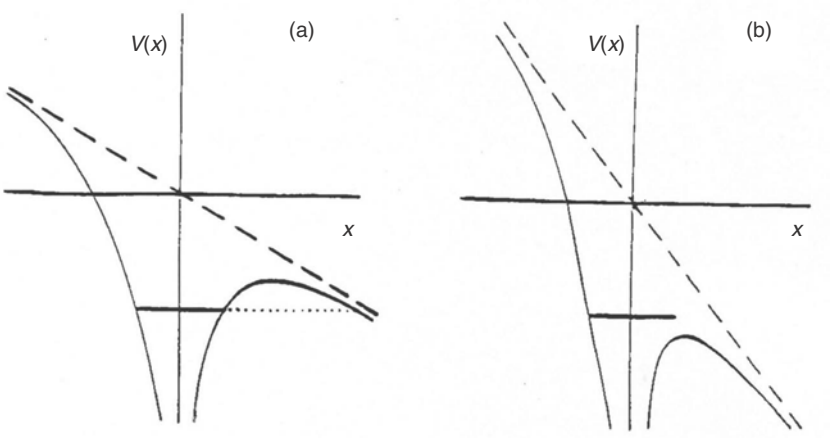

Figure 1.7. One-dimensional model showing (a) tunneling ionization and (b) over-the-barrier ionization. The dashed lines correspond to the contribution to the potential energy due to the instantaneous laser electric field. The solid lines correspond to the full effective potential energy. The position of a bound energy level (in the absence of the laser field) is indicated.

Ammosov, Delone and Krainov [70]. In the case of a hydrogenic system in its ground state, the tunneling rate is given in atomic units by [71]

$$W_{\text{ion}} = \frac{4(2I_{\text{P}})^{5/2}}{\mathcal{E}} \exp\left(-\frac{2(2I_{\text{P}})^{3/2}}{3\mathcal{E}}\right), \tag{1.7}$$

where $\mathcal{E}$ is the static electric field strength. Because of the exponential factor, tunneling occurs predominantly at the peaks of the electric field during the half-cycle when it lowers the potential barrier. As a result, the photoelectron wave packets are emitted in periodic bursts in time. In the energy domain, for sufficiently long pulses, this periodicity gives rise to the ATI spectrum.

A more general quasi-static theory was developed by Keldysh [72] to describe multiphoton ionization in the low-frequency limit, and was pursued by Faisal [73] and Reiss [74]. In the approach of Keldysh, the *strong field approximation* (SFA) is made, whereby it is assumed that an electron, after having being ionized, interacts only with the laser field and not with its parent core. As will be discussed in Chapter 6, an important quantity in this theory is the *Keldysh parameter* γ_{K}, defined as the ratio of the laser and tunneling frequencies, which is given by

$$\gamma_{\text{K}} = \left(\frac{I_{\text{P}}}{2U_{\text{p}}}\right)^{1/2}. \tag{1.8}$$

For $\gamma_{\text{K}} \lesssim 1$, tunneling dynamics dominates, while $\gamma_{\text{K}} \gtrsim 1$ is referred to as the multi-photon ionization regime. It is interesting to note that early evidence of quasi-static

tunneling was found in 1974 by Bayfield and Koch [75] in the microwave ionization of highly excited Rydberg atoms [76].

At low frequencies, as the laser intensity is increased, the barrier in the effective potential becomes narrower and lower, and the sharp ATI peaks of the photoelectron spectra gradually blur into a continuous distribution. Eventually, above a critical intensity I_c (also called "appearance" intensity), the electron can classically "flow over the top" of the barrier (see Fig. 1.7(b)). This is known as "over-the-barrier" ionization (OBI). The approximations based on the tunneling formulae then break down and the atom ionizes quickly. The critical intensity, I_c, at which the maximum of the effective potential is lowered to a value equal to the ionization potential of the bound electron, is $1.4 \times 10^{14}\,\mathrm{W\,cm^{-2}}$ for atomic hydrogen in the ground state and $1.5 \times 10^{15}\,\mathrm{W\,cm^{-2}}$ for helium, also in the ground state. Augst *et al.* [77] and Mevel *et al.* [78] have studied the ionization of noble gases in this intensity regime. As an illustration, the energy spectrum of photoelectrons ejected from helium at the critical intensity I_c and the wavelength $\lambda = 617$ nm, as obtained by Mevel *et al.* [78] is shown in Fig. 1.8.

In order to develop a successful model of strong field phenomena at low frequencies, it is necessary to go beyond tunneling or over-the-barrier ionization, and take into account the possibility that the ionized electron will return to the vicinity of its parent ion or atom core. The semi-classical "recollision model" developed by Corkum [79] and by Kulander, Schafer and Krause [80] is based on the idea that ionization by strong laser fields at low frequencies proceeds via several steps. In the first ("bound–free") step, the active electron is detached from its parent core by tunneling or over-the-barrier ionization. In the second ("free–free") step, the unbound electron interacts mainly with the laser field, so that its dynamics are

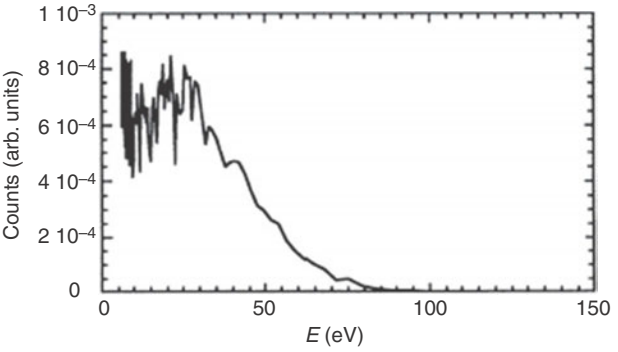

Figure 1.8. Electron energy spectrum from helium at a laser wavelength $\lambda = 617$ nm and the critical intensity $I_c = 1.5 \times 10^{15}\,\mathrm{W\,cm^{-2}}$. The duration of the laser pulse is 100 fs. There is no structure above 30 eV. (From E. Mevel *et al.*, *Phys. Rev. Lett.* **70**, 406 (1993).)

essentially those of a free electron in the field, and can be treated to a good approximation by using classical mechanics. An earlier version of this approach has been used by Kuchiev [81] and van Linden van den Heuvell and Muller [82], and is known as the "simple man's" model of strong field phenomena. As the electric field component of the laser field changes sign, the electron can be accelerated back toward its parent core. If the electron does not return to the core, single ionization will occur. If it does return to the core, then a third step takes place in which a collision of the electron with the core leads to single or multiple ionization while radiative recombination leads to the process of harmonic generation, which will be described in Section 1.4. As we shall see in Chapter 8, the semi-classical "recollision model" has been very useful for explaining a number of novel features observed in multiphoton ionization experiments performed with low-frequency lasers. For example, experiments using kilohertz-repetition rate, high-intensity lasers have allowed precise measurements of photoelectron total yields and energy and angle-differential spectra over many orders of magnitude in yield to be carried out. In particular, the experiments of Paulus *et al.* [83] have revealed the existence of a "plateau" in the ATI photoelectron energy spectra (see Fig. 1.9) which, as we shall see in Chapter 8, is due to recollisions of electrons with their parent cores.

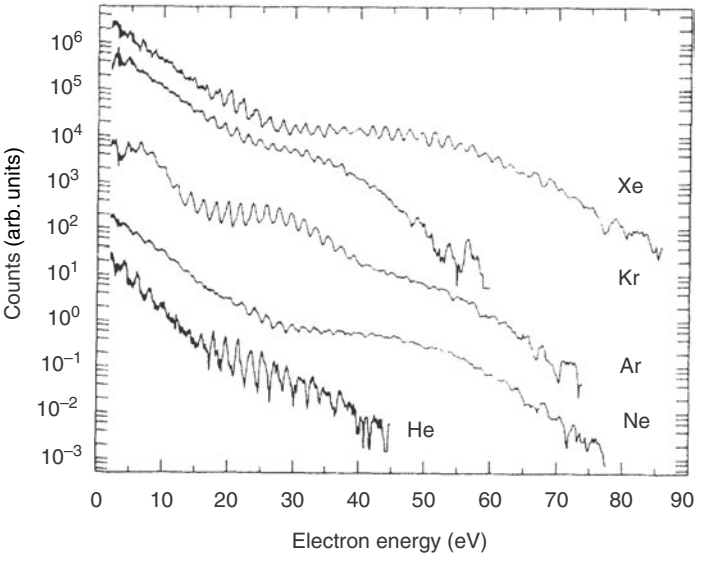

Figure 1.9. Photoelectron counts as a function of photoelectron energy, for various noble gases, at a laser wavelength $\lambda = 630\,\text{nm}$ and an intensity $I \simeq 2 \times 10^{14}\,\text{W cm}^{-2}$ ($3 \times 10^{14}\,\text{W cm}^{-2}$ for He). (From G. G. Paulus *et al.*, *Phys. Rev. Lett.* **72**, 2851 (1994).)

More recently, the investigation of ATI has benefited from the rapid progress made in generating few-cycle laser pulses with peak intensities exceeding the atomic unit I_a. Already at intensities one or more orders of magnitude lower than I_a, atoms can ionize on the time scale of a few optical periods. Hence, the only way to expose atoms to high-intensity laser fields is to irradiate them with the shortest possible laser pulses. Grasbon *et al.* [84] have measured ATI photoelectron spectra for noble gas atoms ionized with intense few-cycle laser pulses. They also found an extended plateau-like structure in the photoelectron energy spectra that can be explained by using the semi-classical recollision model. With respect to the atomic response, the use of sub 10 fs laser pulses makes a significant difference in comparison with 30 fs pulses because all Rydberg states have much longer orbit times than the pulse duration. As a result the REMPI phenomenon, which plays a major role for longer pulses, is much less important for few-cycle pulses.

Using laser pulses having a duration of approximately 6 fs, Paulus *et al.* [85] were able to demonstrate the influence of the carrier-envelope phase (CEP) of an ultra-short pulse on the emission of ATI photoelectrons. They ionized krypton atoms and recorded the photoelectrons with two opposite detectors perpendicular to the laser beam, as illustrated in Fig. 1.10(a). They detected an anticorrelation in the number of electrons emitted to the left or to the right (see Fig. 1.10(b)), which is the signature of the carrier-envelope phase. Indeed, if this phase has a value such that the maximum of the electric field points to the left, more photoelectrons will be counted at the right detector than the left detector. Longer pulses do not exhibit this anticorrelation since the influence of the CEP averages out.

In subsequent work, Paulus *et al.* [47] and Verhoef *et al.* [53] made use of intense few-cycle laser pulses with a stabilized CEP to demonstrate that the direction of emission of ATI photoelectrons can be controlled by varying the CEP of the laser field, thus providing a tool for an accurate determination of the CEP. More recently, Kling *et al.* [56] reported sub-femtosecond control of the electron emission in ATI of the noble gases Ar, Kr and Xe in intense, few-cycle laser fields. Using a velocity-map imaging (VMI) technique, where electrons are projected onto a two-dimensional position-sensitive detector, they were able to measure full-momentum distributions of ATI, and also to determine the CEP from the angular distribution of the emitted electrons.

Let us now consider the multiphoton *double* ionization process

$$n\hbar\omega + A^q \rightarrow A^{q+2} + 2e^-. \tag{1.9}$$

The double ionization of helium from its ground state,

$$n\hbar\omega + \mathrm{He}(1^1\mathrm{S}) \rightarrow \mathrm{He}^{2+} + 2e^-, \tag{1.10}$$

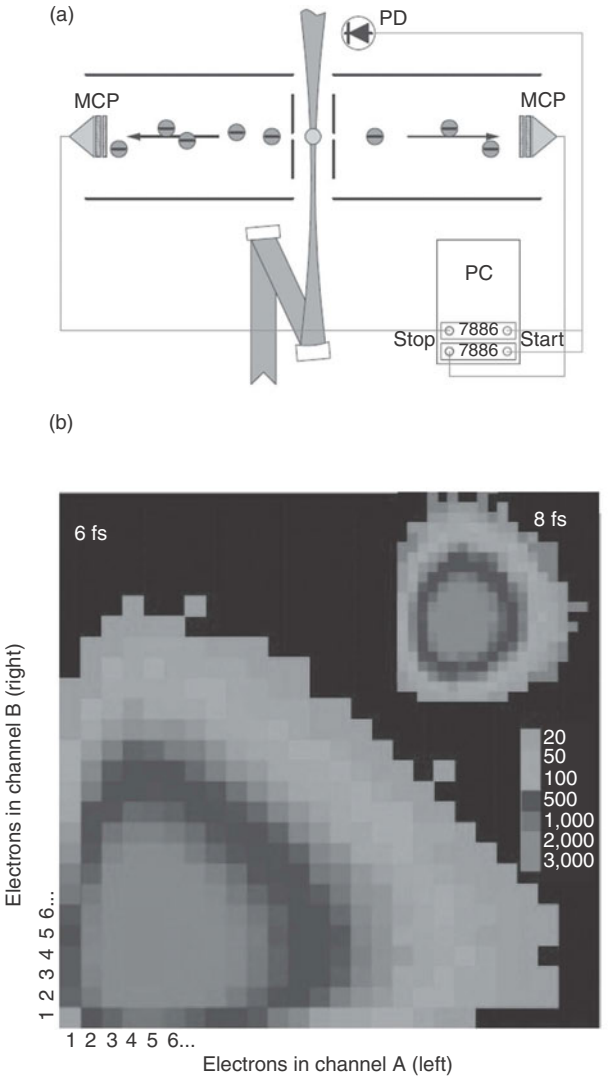

Figure 1.10. (a) Laser pulses of about 6 fs duration are focused onto a gas jet of krypton atoms. The number of electrons emitted to the left and right directions depends on the carrier-envelope phase (CEP) of the laser pulse. They are recorded by two opposite multichannel plate (MCP) detectors perpendicular to the laser beam. The start signal is generated by a fast photodiode (PD) and the electron's time of flight is recorded by a computer (PC). (b) The signature of the carrier-envelope phase is an anticorrelation in the number of electrons emitted to the left or to the right. A graphical representation of the anticorrelation can be obtained by characterizing each laser pulse according to the number of electrons registered in the left and the right detectors. The anticorrelation is manifested in the comparatively high number of laser pulses that produce a strongly asymmetric number of photoelectrons. This leads to contours perpendicular to the diagonal. Longer pulses do not exhibit this anticorrelation, as seen in the upper right corner for a laser pulse of 8 fs duration. (From G. G. Paulus *et al.*, *Nature* **414**, 182 (2001).)

is the most basic of these processes. In 1967, Byron and Joachain [86] proved that in the case of *one*-photon ionization ($n = 1$), the double ionization process (1.10) is very sensitive to *electron correlation effects*. Indeed, this process could not occur in the absence of the electron–electron interaction. The multiphoton case is more complex to analyze. A striking feature of the experimental results obtained by Walker *et al.* [87] is the existence of two distinct intensity regimes (see Fig. 1.11). The first one is at high intensities, where *sequential* double ionization (SDI) dominates in accordance with a "single active electron" (SAE) approximation. The other regime

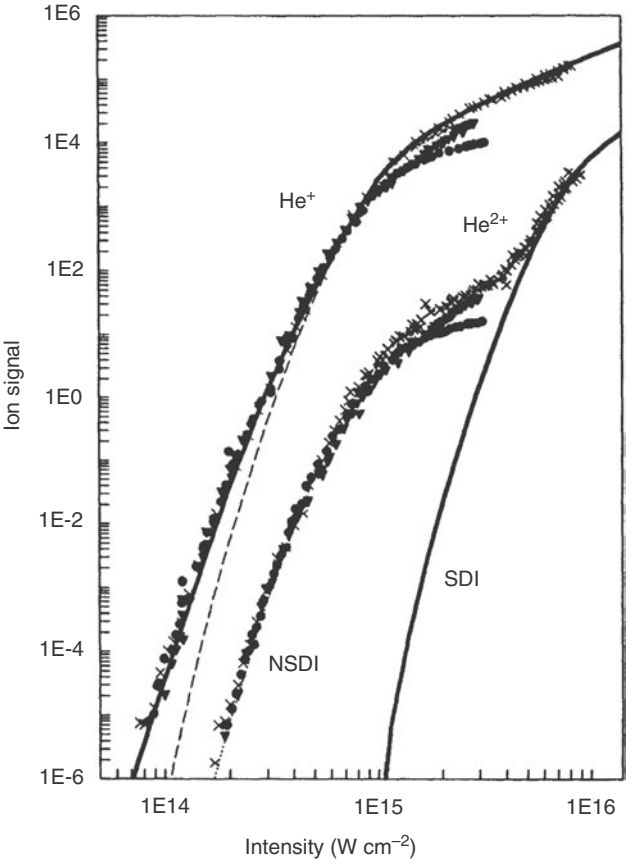

Figure 1.11. Measured He^+ and He^{2+} yields as a function of intensity for linearly polarized laser pulses of wavelength $\lambda = 780$ nm and 160 fs duration. The solid lines show SAE calculations and the dashed line depicts the tunneling theories. The solid curve on the right corresponds to the calculated He^{2+} sequential double ionization (SDI) yield. The symbol NSDI refers to the non-sequential double ionization yield. (From B. Walker *et al., Phys. Rev. Lett.* **73**, 1227 (1994).)

is at lower intensities, where mainly simultaneous double ionization, or in other words *non-sequential* double ionization (NSDI), takes place and the SAE approximation predicts double ionization yields that are several orders of magnitude lower than the experimental data. An important test for theories of multiphoton processes going beyond the SAE approximation (that is, including electron correlation effects) is to calculate accurately double (and, more generally, multiple) ionization yields for multielectron systems in intense laser fields. Advances in experimental techniques based on cold target recoil ion momentum spectroscopy (COLTRIMS) [88] and intense few-cycle laser pulses have allowed multiphoton double ionization to be investigated in more detail [89, 90]. These experimental developments, as well as the theoretical approaches incorporating electron correlation effects, will be discussed in Chapter 8.

1.4 Harmonic generation and attosecond pulses

Matter interacting with a sufficiently intense laser field can emit radiation at higher-order multiples, or *harmonics*, of the angular frequency ω of the "pump" laser. Optical harmonic generation was first observed in a quartz crystal in 1961 by Franken *et al.* [91], who used a ruby laser producing approximately 3 J of 694.3 nm light in a 1 ms pulse, corresponding to an intensity of about $10^6\,\mathrm{W\,cm^{-2}}$, to generate the second harmonic. They pointed out that "the possibility of exploiting this extraordinary intensity for the production of optical harmonics from suitable nonlinear materials is most appealing." Since then, harmonic generation has become a phenomenon used in a variety of applications to extend the range of laser light sources to shorter wavelengths. In the case of atoms interacting with laser pulses comprising many optical cycles and having intensities such that non-dipole and relativistic effects can be neglected, the harmonic angular frequencies Ω are only emitted at odd multiples of the laser angular frequency because of the inversion symmetry of the atom in the field. Hence,

$$\Omega = q\omega, \quad q = 3, 5, \ldots \tag{1.11}$$

When the driving laser pulse comprises only a few optical cycles, the photons are emitted with a continuous distribution of frequencies, not at discrete harmonic frequencies. An effective "harmonic order" is then defined to be the ratio Ω/ω of the angular frequency of the emitted photon to that of the pump laser. High-order harmonic generation (HHG) has attracted considerable interest, since it provides a source of very bright, short-pulse, high-frequency coherent radiation. It has been the subject of several review articles [92–94].

The observation of the third harmonic in noble gases was made in 1967 by New and Ward [95]. Harmonic generation experiments were then performed with long-pulse infra-red lasers [96–98] or ultra-violet pump fields [99-101], but were limited by various effects such as the ionization of the medium or the absorption of the generated radiation in optically thick media.

It was only in the late 1980s that the availability of intense, short-pulse laser fields made it possible to observe high-order harmonics. Experiments performed at the University of Illinois by McPherson *et al.* [102] and Rosman *et al.* [103] showed the generation of up to the 17th harmonic of a 248 nm KrF laser in a neon vapor. At Saclay, Ferray *et al.* [104] observed the harmonic $q = 33$ in argon, and Li *et al.* [105] observed the harmonics $q = 29$ in krypton and $q = 21$ in xenon using a 1064 nm Nd:YAG laser delivering pulses of about 30 ps duration and intensity $3 \times 10^{13}\,\mathrm{W\,cm^{-2}}$. These results were extended in a number of experiments performed with shorter pulses, and at higher intensities [106–112]. For example, Sarukura *et al.* [106] observed the 25th harmonic in He and Ne using a 500 fs, 248 nm KrF laser, a result interpreted as harmonic emission by the ions. Miyazaki and Sakai [107] reported the observation of the 41st harmonic in He with a 800 fs, 616 nm dye laser. In 1993, Macklin, Kmetec and Gordon [108] observed the generation of up to the 109th harmonic in Ne, using a 125 fs, 806 nm Ti:sapphire laser. Also in 1993, L'Huillier and Balcou [109] detected HHG in noble gases, using 1 ps pulses from a Nd:glass laser at intensities around $10^{15}\,\mathrm{W\,cm^{-2}}$. The number of photons recorded per laser pulse in xenon, argon, neon and helium at an intensity $I \simeq 1.5 \times 10^{15}\,\mathrm{W\,cm^{-2}}$ is shown in Fig. 1.12 as a function of the harmonic order. Of special interest is the existence of a plateau of nearly constant conversion efficiency, which is particularly long for helium and neon. We shall see below that non-perturbative theories are required to explain the occurrence of such plateaus. L'Huillier and Balcou detected up to the 135th harmonic in neon at an energy of 160 eV, being then limited by the resolution of their monochromator. The harmonic emission was observed to be directional and of short pulse duration (shorter than the pump pulse). The instantaneous power generated at, for example, 20 eV (the 17th harmonic in Xe) reached about 30 kW, with a conversion efficiency of 10^{-6}. The instantaneous brightness was 10^{22} photons/(Å s), a number which is several orders of magnitude higher than that obtained with conventional light sources in this domain of the electromagnetic spectrum (but of course over a restricted time period).

The use of intense ultra-short laser pulses with peak intensities higher than $10^{15}\,\mathrm{W\,cm^{-2}}$ [34] offers new perspectives for the generation of coherent, tunable, high-frequency (UV or X-ray) pulses by HHG in gases. Atoms or ions exposed to such pulses experience only a few optical cycles, and hence can withstand much stronger laser fields before ionizing than would be possible with longer pulses.

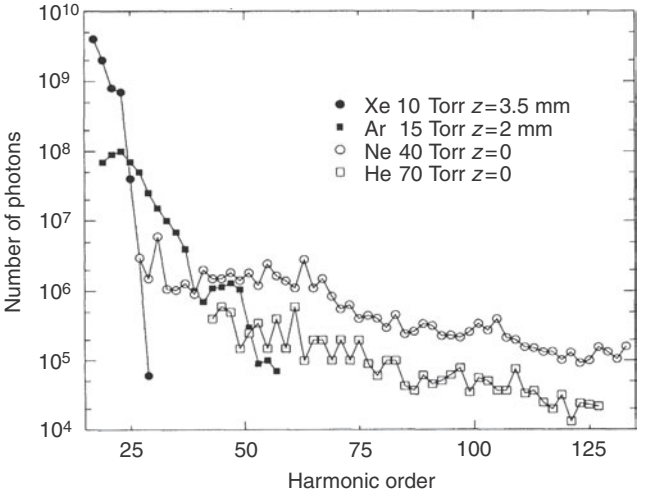

Figure 1.12. Harmonic emission spectra of various noble gases for a "pump" laser of wavelength $\lambda = 1053$ nm and intensity $I \simeq 1.5 \times 10^{15}\,\mathrm{W\,cm^{-2}}$. (From A. L'Huillier and P. Balcou, *Phys. Rev. Lett.* **70**, 774 (1993).)

This in turn permits the generation of photons of much higher energies. The resulting high-frequency laser pulses have durations in the sub-femtosecond range. The highest harmonic frequencies and harmonic orders have been observed under these conditions [113–119]. For example, Chang *et al.* [116] used a Ti:sapphire laser of wavelength $\lambda = 800$ nm delivering pulses of 26 fs duration and peak intensities of about $6 \times 10^{15}\,\mathrm{W\,cm^{-2}}$ to generate coherent soft X-ray harmonics reaching into the water window spectral region around a wavelength of 2.7 nm (corresponding to an energy of 460 eV) in helium, and 5.2 nm (239 eV) in neon. In helium, they observed harmonic peaks up to order $q = 221$ and unresolved harmonic emission up to order $q = 297$. Schnürer *et al.* [117] reported the generation of coherent X-rays with wavelengths down to 2.5 nm (corresponding to an energy of 500 eV) in a helium gas irradiated by sub 10 fs pulses of peak intensity $4 \times 10^{15}\,\mathrm{W\,cm^{-2}}$ generated by a Ti:sapphire laser of wavelength $\lambda = 770$ nm at a 1 kHz repetition rate. In later experiments, Seres *et al.* [118] observed the production of harmonic photons with energies extending to 1.3 keV for helium atoms irradiated by 5 fs pulses, and Chen *et al.* [119] have generated phase-matched high harmonics spanning the water window spectral region.

The theoretical treatment of harmonic generation by an intense laser pulse focused onto a gaseous medium has two main aspects which will be discussed in more detail in Chapter 9. First, the *microscopic single-atom* response to the laser field must be analyzed. Because different atoms in the laser focus experience different peak intensities and phases, the single-atom response must be calculated

over a range of laser field intensity profiles. In order to obtain the *macroscopic* harmonic spectrum generated by the coherent photon emission by all of the atoms in the laser focus, the single-atom responses must be combined by solving Maxwell's equations. In this way propagation and interference effects are accounted for. Unless *phase matching* occurs, these effects can lead to the suppression of the harmonic emission signal.

Let us now consider briefly the theoretical aspects of the problem. The emission of harmonics by the atom is due to the electron oscillations caused by the intense laser field. Let us introduce the *laser-induced atomic dipole moment*

$$\mathbf{d}(t) = \langle \Psi(t)| - e\mathbf{R}|\Psi(t)\rangle, \tag{1.12}$$

which is the expectation value of the electric dipole operator

$$\mathbf{D} = -e\mathbf{R}, \tag{1.13}$$

where

$$\mathbf{R} = \sum_{i=1}^{N} \mathbf{r}_i \tag{1.14}$$

is the sum of the coordinates $\mathbf{r}_i$ of the N atomic electrons. In Equation (1.12), $|\Psi(t)\rangle$ denotes the state vector of the atom in the presence of the laser field. The propagation equations that must be solved to obtain the spectrum of harmonics generated by the medium have source terms which are proportional to the Fourier components, $\mathbf{d}(\Omega)$, of $\mathbf{d}(t)$, namely

$$\mathbf{d}(\Omega) = (2\pi)^{-1/2} \int_{-\infty}^{\infty} \exp(-\mathrm{i}\Omega t)\, \mathbf{d}(t)\, \mathrm{d}t. \tag{1.15}$$

Due to phase matching effects, the strength of the harmonics emitted by the medium may vary with Ω in a different way than $|\mathbf{d}(\Omega)|^2$. For the case of a single atom, the emitted power spectrum is proportional to the quantity $|\mathbf{a}(\Omega)|^2$, where

$$\mathbf{a}(\Omega) = (2\pi)^{-1/2} \int_{-\infty}^{\infty} \exp(-\mathrm{i}\Omega t)\, \mathbf{a}(t)\, \mathrm{d}t \tag{1.16}$$

is the Fourier transform of the acceleration of the laser-induced atomic dipole moment,

$$\mathbf{a}(t) = \frac{\mathrm{d}^2}{\mathrm{d}t^2}\mathbf{d}(t) \equiv \ddot{\mathbf{d}}(t). \tag{1.17}$$

For weak laser fields, the harmonic emission rates can be calculated by the perturbation theory which will be developed in Chapter 3. It is then found that in general the harmonic intensity decreases from one order to the next. In contrast, we

note from Fig. 1.12 that at high laser intensities, and for linearly polarized pump fields, the harmonic intensity distribution exhibits a rapid decrease over the first few harmonics, followed by a plateau of approximately constant intensity, and then a cut-off corresponding to an abrupt decrease of harmonic intensity. The existence of the plateau can only be explained by using non-perturbative approaches. In particular, by solving numerically the time-dependent Schrödinger equation (TDSE), Krause, Schafer and Kulander [120] found that the cut-off angular frequency ω_c of the harmonic spectrum is given approximately by

$$\omega_c \simeq (I_P + 3U_p)/\hbar. \tag{1.18}$$

Using the semi-classical recollision model [79, 80], it will be shown in Chapter 6 that the maximum kinetic energy of a classical electron recolliding with the atomic core is $3.17U_p$, so that the highest energy that can be radiated is $I_P + 3.17U_p$, in good agreement with the TDSE calculations and with experiment. A quantum-mechanical theory of HHG, based on a low-frequency strong-field approximation (SFA), has been developed by Lewenstein *et al.* [121, 122] and will be discussed in Chapter 6. It embodies the semi-classical recollision model, and also accounts for quantum effects such as tunneling ionization, wave-packet spreading and interferences.

It also follows from the SFA that the Fourier component of the induced atomic dipole moment corresponding to the qth harmonic has a phase, denoted by ϕ_q, that in first approximation is proportional to the product $U_p\tau$, where τ is the time spent by the ionized electron in the continuum before it returns and recombines radiatively with its parent ion. Using Equation (1.5), we see that the phase ϕ_q is a linear function of the intensity, with a slope depending on the time τ. The main contributions to the emission of each harmonic in the plateau region come from two electron trajectories. Electrons following these two trajectories have the same kinetic energy when they return to the atomic core. The two trajectories are referred to, respectively, as the "short" trajectory and "long" trajectory. The corresponding times spent by the electron in the continuum, τ_1 and τ_2, are shorter than one laser field period $T = 2\pi/\omega$, so that

$$0 < \tau_1 < \tau_2 < T. \tag{1.19}$$

The variation of the dipole phase ϕ_q with intensity, in the strong-field regime, plays an important role in the macroscopic aspect of harmonic emission [93].

An important new development is the possibility of using high-order harmonics to generate laser pulses having durations in the attosecond (10^{-18} s) range. This subject has been reviewed by Agostini and DiMauro [123], Scrinzi *et al.* [124], Niikura and Corkum [125] and Krausz and Ivanov [126]. Fourier synthesis was proposed by Hänsch [127], by Farkas and Toth [128] and by Harris, Macklin and

Hänsch [129] as a method to produce pulses having durations of a few attoseconds. The basic idea is to generate a "comb" of equidistant frequencies with controlled relative phases. The principle is analogous to that of the mode-locked laser [130]: if N spectral modes within the gain bandwidth are phase-locked, then the temporal profile is a sequence of pulses separated by the cavity round-trip time, each with a duration proportional to N^{-1}. Several methods using non-linear processes to obtain a wide sequence of equidistant frequencies have been proposed. Hänsch [127] suggested using sum and frequency mixing to generate six frequencies, while Farkas and Toth [128] recognized that high harmonic generation in atoms could readily produce a comb of odd-order harmonics of nearly equal amplitudes over a large frequency range within the plateau region. A similar idea was proposed by Harris, Macklin and Hänsch [129]. If these harmonics were emitted in phase, the corresponding temporal profile (which is the Fourier transform of the periodic spectrum of the harmonics) would consist of a train of ultra-short pulses separated by half the laser period, the duration of each pulse being proportional to the inverse of the number of harmonics. However, calculations of the single-atom response, performed by Antoine, L'Huillier and Lewenstein [131], showed that the harmonics in the plateau region were in general not in phase, due to the interference of various energetically allowed electronic trajectories leading to the harmonic emission. In fact, in the plateau region there are at least two trajectories per half laser field period (in particular the short one and the long one) that lead to the emission of a given harmonic. As a result, the temporal profile exhibits two dominant peaks per half-period of the laser field that can be attributed to these trajectories. This is illustrated in Fig. 1.13, where the single-atom response for the temporal superposition of harmonics 41 to 61 generated in neon calculated by Antoine, L'Huillier and Lewenstein [131] is shown. However, Antoine, L'Huillier and Lewenstein also showed that the propagation in the atomic medium could select one of these trajectories. Indeed, under certain conditions, phase matching strongly depends on the phase ϕ_q, which exhibits a different intensity dependence for the different trajectories, as mentioned above. For example, as illustrated in Fig. 1.13, Antoine, L'Huillier and Lewenstein found that the macroscopic temporal profile for laser focusing before the gas jet – which selects the short electron trajectories – yields a single peak, of 300 as duration, per half-period of the laser field. This prediction has been confirmed qualitatively by a measurement of the relative phases of a group of harmonics generated in argon [132]. The phases are consistent with the emission of a train of 250 as pulses.

The generation of a *train* of attosecond pulses by Fourier synthesis of harmonics does not require particularly short pump laser pulses. However, for many applications, it is desirable to obtain *isolated* attosecond pulses. A first method, proposed by Corkum, Burnett and Ivanov [133], Ivanov *et al.* [134] and Platonenko and

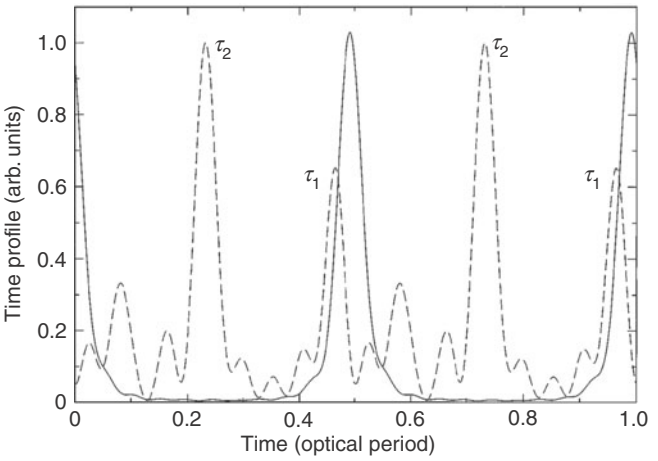

Figure 1.13. Theoretical harmonic intensity time profile obtained by summing the ten harmonics between the 41st to the 61st (solid line) emitted by a gas jet located before the laser focus. The peak intensity of the driving laser pulse is $6.6 \times 10^{14}\,\mathrm{W\,cm^{-2}}$. The dashed line denotes the corresponding single-atom response. The labels τ_1 and τ_2 refer to the short and the long electron trajectories, respectively. The figure shows that the intensity peaks corresponding to the long electron trajectories are suppressed during propagation through the atomic medium. (From P. Antoine, A. L'Huillier and M. Lewenstein, *Phys. Rev. Lett.* **77**, 1234 (1996).)

Strelkov [135], uses the high sensitivity of the harmonic efficiency to the laser field polarization [136], and is therefore called *polarization gating*. It follows from the three-step recollision model that harmonics are essentially produced when the polarization of the laser field is linear. Indeed, the probability of an ionized electron returning to its parent ion is significantly reduced when the laser field is no longer linearly polarized. By creating a laser pulse whose polarization is linear only during a short time (close to a laser period) the harmonic emission may be limited to this interval, so that single attosecond pulses are produced. There are different techniques for implementing a polarization gate. For example, using two chirped laser pulses delayed in time, Altucci *et al.* [137] have reduced photon emission to a few femtoseconds. Using two delayed counter-circularly polarized laser pulses, a temporal gating has also been demonstrated [138–140].

A second method to obtain isolated attosecond pulses from HHG is to use an ultra-short few-cycle pump pulse. Theoretical calculations have predicted the possibility of generating a single XUV burst [34, 141]. Using few-cycle (<7 fs) linearly polarized laser pump pulses with stabilized carrier-envelope phase, isolated attosecond pulses have been produced by selecting the high-energy (cut-off) harmonics ($\sim$90 eV) generated in neon [48, 142, 143].

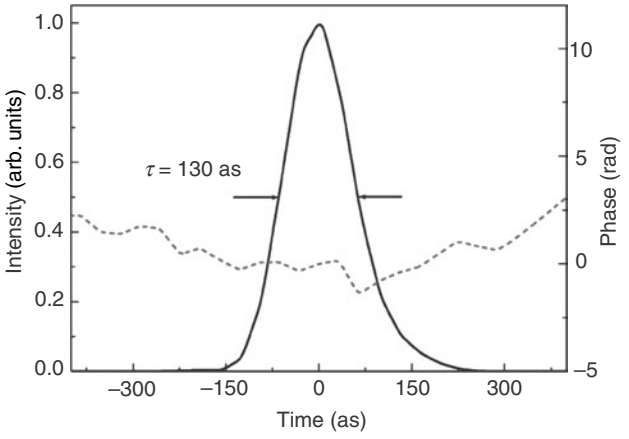

Figure 1.14. Reconstruction of the temporal intensity profile (solid curve) and phase (dotted curve) of the attosecond pulses generated using 5 fs laser pulses ($\lambda = 750$ nm) with stabilized carrier-envelope phase interacting with Ar atoms. (From G. Sansone *et al.*, *Science* **314**, 443 (2006).)

Another approach for generating isolated attosecond pulses uses a combination of the two aforementioned methods. It is based on the use of phase-stabilized few-cycle driving pulses in combination with the polarization gating technique. Sansone *et al.* [144] have generated in this way single-cycle isolated 130 as pulses around 36 eV by using 5 fs driving pulses, as shown in Fig. 1.14.

Let us now consider photon emission by *positive ions* interacting with very intense, ultra-short (few-cycle) pulses. Positive ions can survive higher laser intensities because of their higher binding energies, and can therefore emit more energetic photons [112, 145–147]. However, the HHG conversion efficiency begins to decrease as the laser intensity increases. This is a consequence of non-dipole effects, due essentially to the magnetic field component of the laser field [148–152]. As an illustration, we show in Fig. 1.15 the magnitude squared of the Fourier transform of the dipole acceleration of a Be^{3+} ion as a function of the emitted photon energy (in units of $\hbar\omega$) for an 800 nm four-cycle laser pulse with a peak intensity of 3.6×10^{17} W cm^{-2}. The influence of the magnetic field on photon emission polarized along the polarization direction of the laser field (taken to be the x-axis) can be seen by comparing the dipole and non-dipole results. This reduction is easy to understand within the semi-classical three-step recollision model: the magnetic field component of the laser pulse induces a displacement of the electron along the laser field propagation direction which causes returning electrons to "miss" the core. Another non-dipole effect is the emission of photons polarized along the laser field propagation direction (taken to be the z-axis), which is forbidden in the dipole

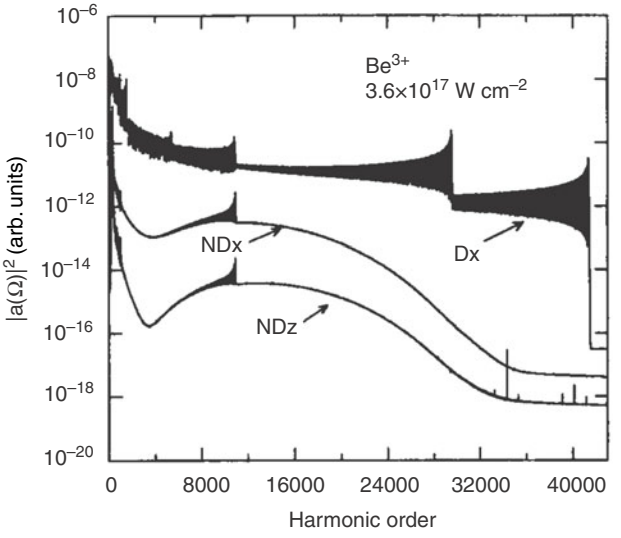

Figure 1.15. Magnitude squared of the Fourier transform of the SFA dipole acceleration (in arbitrary units) of Be^{3+} as a function of the harmonic order (the emitted photon energy in units of laser photon energy). Dipole results (Dx) are shown, as well as non-dipole results for photons polarized along the laser field polarization direction $\hat{\mathbf{x}}$ (NDx) and polarized along the laser field propagation direction $\hat{\mathbf{z}}$ (NDz). The incident laser pulse has a total duration of four optical cycles, a carrier wavelength of 800 nm and a peak intensity of $3.6 \times 10^{17}\,\mathrm{W\,cm^{-2}}$. (From C. J. Joachain, N. J. Kylstra and R. M. Potvliege, *J. Mod. Opt.* **50**, 313 (2003).)

approximation. As seen from Fig. 1.15, this emission is typically two orders of magnitude lower than emission along the laser field polarization direction.

1.5 Laser-assisted electron–atom collisions

An electron scattered by an atom in the presence of a laser field can absorb or emit radiation. Since these radiative collisions involve continuum states of the electron–atom system, they are often called "free–free transitions" (FFT). In weak laser fields, only one-photon processes have a large enough probability to be observed. However, as the field strength is increased, multiphoton processes become important. Examples of laser-assisted electron–atom collisions are "elastic" collisions:

$$\mathrm{e}^- + \mathrm{A}(i) + n\hbar\omega \rightarrow \mathrm{e}^- + \mathrm{A}(i); \tag{1.20}$$

inelastic collisions:

$$\mathrm{e}^- + \mathrm{A}(i) + n\hbar\omega \rightarrow \mathrm{e}^- + \mathrm{A}(f); \tag{1.21}$$

and single ionization (e, 2e) collisions:

$$e^- + A(i) + n\hbar\omega \rightarrow A^+(f) + 2e^-, \tag{1.22}$$

where $A(i)$ and $A(f)$ denote an atom or ion A in the initial state i and the final state f, respectively, and $A^+(f)$ means the A^+ ion in the final state f. Positive values of n correspond to photon absorption (inverse bremsstrahlung), negative ones to photon emission (stimulated bremsstrahlung) and $n = 0$ to a collision process in the laser field without net absorption or emission of photons. In contrast to *laser-induced* processes, such as multiphoton ionization and harmonic generation, *laser-assisted* processes can take place in the absence of the laser field, but are modified by its presence. Reviews of laser-assisted electron–atom collisions have been given by Gavrila [153], Francken and Joachain [154], Mason [155], Joachain [17] and Ehlotzky, Jaron and Kaminski [156].

Information on laser-assisted electron–atom collision processes is obtained by performing three-beam experiments, in which an atomic beam is crossed in coincidence by a laser beam and an electron beam, and the scattered electrons are detected. It is worth pointing out that the laser intensity should not be too high ($I < I_a$), since otherwise the atom would be ionized. Several experiments of this kind have been carried out, in which the exchange of photons between the electron–atom system and the laser field has been observed in laser-assisted elastic [157–159], inelastic [160, 161] and ionization processes [162]. As an illustration, we show in Fig. 1.16 the results of Weingartshofer *et al.* [158] for laser-assisted elastic electron–argon scattering. Even at the modest intensity of $10^8\,\mathrm{W\,cm^{-2}}$, as many as 11 photon emission and absorption transitions were observed. As seen from Fig. 1.16, the relative intensities of two successive peaks are of the same order of magnitude, which indicates that perturbation theory cannot be used to analyze these results.

A detailed treatment of laser-assisted electron–atom collisions will be given in Chapter 10. We remark that this problem is in general very complex, not only from the experimental point of view, but also on the theoretical side. Indeed, in addition to the difficulties associated with the treatment of field-free electron–atom collisions, the presence of the laser field introduces new parameters (laser frequency, intensity, polarization,...) which influence the collision. It is therefore of interest to consider a much simpler problem in which the target atom is modeled by a center of force, namely a static potential, and hence does not exhibit any internal structure. Within the framework of this model, general expressions for the required collision cross sections can be obtained [163, 164], and the first Born approximation result of Bunkin and Fedorov [165] as well as the low-frequency (or soft-photon) approximation of Kroll and Watson [166] derived.

As in the field-free case [167, 168], the theoretical treatment of electron collisions with real atoms in the presence of a laser field depends on the energy of the projectile

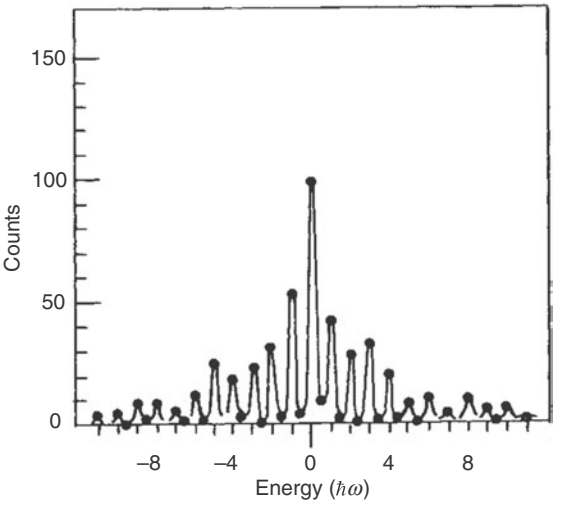

Figure 1.16. Energy spectrum of electrons scattered by argon atoms in the presence of a laser field of photon energy $\hbar\omega = 0.117$ eV and intensity $I = 10^8$ W cm^{-2} from a CO_2 laser. The circles correspond to the experimental data; the full line is drawn to guide the eye. The abscissa gives the final electron energy in units of the photon energy, with the origin fixed at the initial electron energy of 15.8 eV. The scattering angle $\theta = 155°$. (From A. Weingartshofer *et al.*, *J. Phys. B* **16**, 1805 (1983).)

electron. For fast incident electrons, having an energy of at least 100 eV, the semi-perturbative theory of Byron and Joachain [169] can be applied. In this approach, the interaction of the laser field with the unbound electron(s) is treated "exactly." On the other hand, the projectile electron–target atom interaction is treated perturbatively by using the Born series [167]. Finally, the interaction of the laser field with the target atom, responsible for *target-dressing effects*, can be treated perturbatively for laser intensities $I < I_a$ and for non-resonant processes.

For slow incident electrons, a fully non-perturbative treatment is required. The R-matrix–Floquet theory [10, 11] provides such a treatment. We point out that the semi-perturbative theory mentioned above and the R-matrix–Floquet theory are complementary. The former breaks down for slow incident electrons, where the Born series cannot be used to treat the electron–atom interaction. The latter is difficult to apply for fast incident electrons, where many partial waves are required to calculate the cross sections.

References

[1] A. Einstein, *Annalen der Physik* **17**, 132 (1905).
[2] G. N. Lewis, *Nature* **118**, 132 (1926).
[3] M. Göppert-Mayer, *Ann. Phys.* **9**, 273 (1931).
[4] C. J. Joachain and N. J. Kylstra, *Laser Phys.* **11**, 212 (2001).

[5] C. J. Joachain, N. J. Kylstra and R. M. Potvliege, *J. Mod. Opt.* **50**, 313 (2003).
[6] Y. I. Salamin, S. X. Hu, K. Z. Hatsagortsyan and C. H. Keitel, *Phys. Rep.* **427**, 41 (2006).
[7] A. Maquet, R. Taïeb and V. Véniard, Relativistic laser-atom physics. In T. Brabec, ed., *Strong Field Laser Physics*, Springer Series in Optical Sciences 134 (New York: Springer, 2009), p. 477.
[8] A. Maquet, S. I. Chu and W. P. Reinhardt, *Phys. Rev. A* **27**, 2946 (1983).
[9] R. M. Potvliege and R. Shakeshaft, *Phys. Rev. A* **38**, 1098 (1988).
[10] P. G. Burke, P. Francken and C. J. Joachain, *Europhys. Lett.* **13**, 617 (1990).
[11] P. G. Burke, P. Francken and C. J. Joachain, *J. Phys. B* **24**, 761 (1991).
[12] K. C. Kulander, *Phys. Rev. A* **36**, 2726 (1987).
[13] H. G. Muller, *Phys. Rev. A* **60**, 1341 (1999).
[14] M. Gavrila, ed., *Atoms in intense laser fields, Adv. At. Mol. Phys. Suppl.* **1** (1992).
[15] T. Brabec, ed., *Strong Field Laser Physics*, Springer Series in Optical Science 134 (New York: Springer, 2009).
[16] K. Burnett, V. C. Reed and P. L. Knight, *J. Phys. B* **26**, 561 (1993).
[17] C. J. Joachain, Theory of laser-atom interactions. In R. M. More, ed., *Laser Interactions with Atoms, Solids and Plasmas* (New York: Plenum Press, 1994), p. 39.
[18] K. C. Kulander and M. Lewenstein, *Springer Handbook of Atomic, Molecular and Optical Physics*, chapter Multiphoton and Strong-Field Processes (New York: Springer Science, 2006), p. 1077.
[19] M. Protopapas, C. H. Keitel and P. L. Knight, *Rep. Progr. Phys.* **60**, 389 (1997).
[20] C. J. Joachain, M. Dörr and N. J. Kylstra, *Adv. At. Mol. Opt. Phys.* **42**, 225 (2000).
[21] D. B. Milosevic and F. Ehlotzky, *Adv. At. Mol. Opt. Phys.* **49**, 373 (2003).
[22] F. H. M. Faisal, *Theory of Multiphoton Processes* (New York: Plenum Press, 1987).
[23] M. H. Mittleman, *Introduction to the Theory of Laser–Atom Interactions*, 2nd edn (New York: Plenum Press, 1993).
[24] N. B. Delone and V. P. Krainov, *Multiphoton Processes in Atoms* (Berlin: Springer-Verlag, 1999).
[25] F. Grossmann, *Theoretical Femtosecond Physics* (Berlin: Springer-Verlag, 2008).
[26] D. Strickland and G. Mourou, *Opt. Commun.* **56**, 219 (1985).
[27] G. A. Mourou, T. Tajima, and S. V. Bulanov, *Rev. Mod. Phys.* **78**, 309 (2006).
[28] S. Bahk, P. Rousseau, T. A. Planchon *et al.*, *Optics Lett.* **29**, 2837 (2004).
[29] A. Dubietis, G. Jonusauskas and A. Piskarkas, *Opt. Commun.* **88**, 437 (1992).
[30] I. N. Ross, P. Matousek, M. Towrie, A. J. Langley and J. L. Collier, *Opt. Commun.* **144**, 125 (1997).
[31] R. A. Baumgartner and R. L. Byer, *IEEE J. Quantum Electron.* **QE-15(6)**, 432 (1979).
[32] I. N. Ross, Optical parametric amplification techniques. In T. Brabec, ed., Strong Field Laser Physics, *Springer Series in Optical Sciences* 134 (New York: Springer, 2009), p. 35.
[33] P. Meystre and M. Sargent III, *Elements of Quantum Optics* (Berlin: Springer-Verlag, 1990).
[34] T. Brabec and F. Krausz, *Rev. Mod. Phys.* **72**, 545 (2000).
[35] U. Keller, *Nature* **424**, 831 (2003).
[36] M. Nisoli, S. Stagira, S. De Silvestri *et al. Appl. Phys. B* **65**, 189 (1997).
[37] S. Sartania, Z. Cheng, M. Lenzner *et al. Optics Lett.* **22**, 1562 (1997).
[38] M. Nisoli, S. De Silvestri and O. Svelto, *Appl. Phys. Lett.* **68**, 2793 (1996).
[39] R. Szipöcs, K. Ferencz, C. Spielmann and F. Krausz, *Opt. Lett.* **19**, 201 (1994).
[40] C. P. Hauri, P. Schlup, G. Arisholm, J. Biegert and U. Keller, *Opt. Lett.* **29**, 1369 (2004).

[41] R. T. Zinkstok, S. Witte, W. Hogervorst and K. S. E. Eikema, *Opt. Lett.* **30**, 78 (2005).
[42] N. Ishii, L. Turi, V. S. Yakovlev *et al.*, *Opt. Lett.* **30**, 567 (2005).
[43] S. Witte, R. T. Zinkstok, W. Hogervorst and K. S. E. Eikema, *Opt. Express* **13**, 4903 (2005).
[44] S. T. Cundiff, F. Krausz and T. Fuji, Carrier-envelope phase of ultrashort pulses. In T. Brabec, ed., *Strong Field Laser Physics*, Springer Series in Optical Sciences 134 (New York: Springer, 2009), p. 61.
[45] D. J. Jones, S. A. Diddams, J. K. Ranka *et al.*, *Science* **288**, 635 (2000).
[46] A. Apolonski, A. Poppe, G. Tempea *et al.*, *Phys. Rev. Lett.* **85**, 740 (2000).
[47] G. G. Paulus, F. Lindner, H. Walther *et al.*, *Phys. Rev. Lett.* **91**, 253004 (2003).
[48] A. Baltuška, T. Udem, M. Uiberacker *et al.*, *Nature* **421**, 611 (2003).
[49] E. Goulielmakis, M. Uiberacker, R. Kienberger *et al.*, *Science* **305**, 1267 (2004).
[50] A. Apolonski, P. Dombi, G. G. Paulus *et al.*, *Phys. Rev. Lett.* **92**, 073902 (2004).
[51] T. Fuji, J. Rauschenberger, C. Gohle *et al.*, *New J. Phys.* **7**, 116 (2005).
[52] E. Gagnon, I. Thomann, A. Paul *et al.*, *Opt. Lett.* **31**, 1866 (2006).
[53] A. Verhoef, A. Fernández, M. Lezius, K. O'Keeffe, M. Uiberacker and F. Krausz, *Opt. Lett.* **31**, 3520 (2006).
[54] M. Kress, T. Loffler, M. D. Thomson *et al.*, *Nat. Phys.* **2**, 327 (2006).
[55] C. Haworth, L. Chipperfield, J. Robinson, P. Knight, J. Marangos and J. Tisch, *Nat. Phys.* **3**, 52 (2007).
[56] M. F. Kling, J. Rauschenberger, A. Verhoef *et al.*, *New J. Phys* **10**, 025024 (2008).
[57] T. Fuji, N. Ishii, C. Y. Teisset *et al.*, *Opt. Lett.* **31**, 1103 (2006).
[58] D. Batani, C. J. Joachain, S. Martellucci and A. N. Chester, eds, *Atoms, Solids and Plasmas in Super-Intense Laser Fields*, (New York: Kluwer Academic – Plenum Publishers, 2001).
[59] D. Batani, C. J. Joachain and S. Martellucci, eds, *Atoms and Plasmas in Super-Intense Laser Fields*, vol. 88 (Bologna: Italian Physical Society, 2004).
[60] J. Feldhaus and B. Sonntag, Free-electron lasers – high-intensity X-ray sources. In T. Brabec, ed., *Strong Field Laser Physics*, Springer Series in Optical Sciences 134 (New York: Springer, 2009), p. 91.
[61] D. A. G. Deacon, L. R. Elias, J. M. J. Madley, G. J. Ramian, H. A. Schwettman and T. I. Smith, *Phys. Rev. Lett.* **38**, 892 (1977).
[62] J. Andruszkow, B. Aune, V. Ayvazyan *et al.*, *Phys. Rev. Lett.* **85**, 3825 (2000).
[63] V. Ayvazyan, N. Baboi, I. Bohnet *et al.*, *Phys. Rev. Lett.* **88**, 104802 (2002).
[64] E. K. Damon and R. G. Tomlinson, *Appl. Opt.* **2**, 546 (1963).
[65] G. S. Voronov and N. B. Delone, *Sov. Phys. JETP Lett.* **1**, 66 (1965).
[66] J. L. Hall, E. J. Robinson and L. M. Branscomb, *Phys. Rev. Lett.* **14**, 1013 (1965).
[67] P. Agostini, F. Fabre, G. Mainfray, G. Petite and N. K. Rahman, *Phys. Rev. Lett.* **42**, 1127 (1979).
[68] G. Petite, P. Agostini and H. G. Muller, *J. Phys. B* **21**, 4097 (1988).
[69] R. R. Freeman, P. H. Bucksbaum, H. Milchberg, S. Darack, D. Schumacher and M. E. Geusic, *Phys. Rev. Lett.* **59**, 1092 (1987).
[70] M. V. Ammosov, N. B. Delone and V. P. Krainov, *Sov. Phys. JETP* **64**, 1191 (1986).
[71] L. D. Landau and E. M. Lifshitz, *Quantum Mechanics* (Reading, Mass.: Addison Wesley, 1958).
[72] L. V. Keldysh, *Sov. Phys. JETP* **20**, 1307 (1965).
[73] F. H. M. Faisal, *J. Phys. B* **6**, L89 (1973).
[74] H. R. Reiss, *Phys. Rev. A* **22**, 1786 (1980).
[75] J. E. Bayfield and P. M. Koch, *Phys. Rev. Lett.* **33**, 258 (1974).
[76] T. F. Gallagher, *Rydberg Atoms* (Cambridge: Cambridge University Press, 1984).

[77] S. Augst, D. Strickland, D. Meyerhofer, S. L. Chin and J. H. Eberly, *Phys. Rev. Lett.* **63**, 2212 (1989).
[78] E. Mevel, P. Breger, R. Trainham *et al.*, *Phys. Rev. Lett.* **70**, 406 (1993).
[79] P. B. Corkum, *Phys. Rev. Lett.* **71**, 1994 (1993).
[80] K. C. Kulander, K. J. Schafer and J. L. Krause. In B. Piraux, A. L'Huillier, and K. Rzążewski, eds, *Super-Intense Laser-Atom Physics* (New York: Plenum Press, 1993), p. 95.
[81] M. Y. Kuchiev, *JETP Lett.* **45**, 404 (1987).
[82] H. B. van Linden van den Heuvell and H. G. Muller. In S. J. Smith and P. L. Knight, eds., *Multiphoton Processes*, (Cambridge: Cambridge University Press, 1988).
[83] G. G. Paulus, W. Nicklich, H. Xu, P. Lambropoulos and H. Walther, *Phys. Rev. Lett.* **72**, 2851 (1994).
[84] F. Grasbon, G. G. Paulus, H. Walther *et al.*, *Phys. Rev. Lett.* **91**, 173003 (2003).
[85] G. G. Paulus, F. Grasbon, H. Walther *et al.*, *Nature* **414**, 182 (2001).
[86] F. W. Byron and C. J. Joachain, *Phys. Rev.* **164**, 1 (1967).
[87] B. Walker, B. Sheehy, L. F. DiMauro, P. Agostini, K. J. Schafer and K. Kulander, *Phys. Rev. Lett.* **73**, 1227 (1994).
[88] J. Ullrich, R. Moshammer, A. Dorn, R. Dörner, L. P. Schmidt and H. Schmidt-Böcking, *Rep. Prog. Phys.* **66**, 1463 (2003).
[89] A. Rudenko, K. Zrost, B. Feuerstein *et al.*, *Phys. Rev. Lett.* **93**, 253001 (2004).
[90] X. Liu, H. Rottke, E. Eremina *et al.*, *Phys. Rev. Lett.* **93**, 263001 (2004).
[91] P. A. Franken, A. E. Hill, C. W. Peters and G. Weinreich, *Phys. Rev. Lett.* **7**, 118 (1961).
[92] A. L'Huillier, L. A. Lompré, G. Mainfray and C. Manus, *Adv. At. Mol. Opt. Phys. Suppl.* **1**, 139 (1992).
[93] P. Salières, A. L'Huillier, P. Antoine and M. Lewenstein, *Adv. At. Mol. Opt. Phys.* **41**, 83 (1999).
[94] P. Salières, In D. Batani, C. J. Joachain and S. Martellucci, eds. *Atoms and Plasmas in Super-Intense Laser Fields*, vol. 88 (Bologna: Italian Physical Society, 2004), p. 303.
[95] G. H. C. New and J. F. Ward, *Phys. Rev. Lett.* **19**, 556 (1967).
[96] D. I. Metchkov, V. M. Mitev, L. I. Pavlov and K. V. Stamenov, *Opt. Commun.* **21**, 391 (1977).
[97] M. G. Groseva, D. I. Metchkov, V. M. Mitev, L. I. Pavlov and K. V. Stamenov, *Opt. Commun.* **23**, 77 (1977).
[98] J. Wildenauer, *J. Appl. Phys.* **62**, 41 (1987).
[99] J. Reintjes, C. Y. She and R. C. Eckard, *IEEE J. Quantum Electron.* **QE-14**, 581 (1978).
[100] J. Reintjes, L. L. Tankersley and R. Christensen, *Opt. Commun.* **39**, 334 (1981).
[101] J. Bokor, P. H. Bucksbaum and R. R. Freeman, *Opt. Lett.* **8**, 217 (1983).
[102] A. McPherson, G. Gibson, H. Jara *et al.*, *J. Opt. Soc. Am. B* **4**, 595 (1987).
[103] R. Rosman, G. Gibson, K. Boyer *et al.*, *J. Opt. Soc. Am. B* **5**, 1237 (1988).
[104] M. Ferray, A. L'Huillier, X. F. Li, L. A. Lompré, G. Mainfray and C. Manus, *J. Phys. B* **21**, L31 (1988).
[105] X. F. Li, A. L'Huillier, M. Ferray, L. A. Lompré and G. Mainfray, *Phys. Rev. A* **39**, 5751 (1989).
[106] N. Sarukura, K. Hata, T. Adachi, R. Nodomi, M. Watanabe and S. Watanabe, *Phys. Rev. A* **43**, 1669 (1991).
[107] K. Miyazaki and H. Sakai, *J. Phys. B* **25**, L83 (1992).
[108] J. J. Macklin, J. D. Kmetec and C. L. Gordon, *Phys. Rev. Lett.* **70**, 766 (1993).

[109] A. L'Huillier and P. Balcou, *Phys. Rev. Lett.* **70**, 774 (1993).
[110] K. Miyazaki and H. Takada, *Phys. Rev. A* **52**, 3007 (1995).
[111] Y. Nagata, K. Midorikawa, M. Obara and K. Toyoda, *Opt. Lett.* **21**, 15 (1996).
[112] S. G. Preston, A. Sampera, M. Zepf *et al.*, *Phys. Rev. A* **53**, R31 (1996).
[113] J. Zhou, J. Peatross, M. M. Murnane, H. C. Kapteyn and I. P. Christov, *Phys. Rev. Lett.* **76**, 752 (1996).
[114] I. P. Christov, J. P. Zhou, J. Peatross, A. Rundquist, M. M. Murnane and H. C. Kapteyn, *Phys. Rev. Lett.* **77**, 1743 (1996).
[115] C. Spielmann, N. H. Burnett, S. Sartania *et al.*, *Science* **278**, 661 (1997).
[116] Z. Chang, A. Rundquist, H. Wang, M. M. Murnane and H. C. Kapteyn, *Phys. Rev. Lett.* **79**, 2967 (1997).
[117] M. Schnürer, C. Spielmann, P. Wobrauschek *et al.*, *Phys. Rev. Lett.* **80**, 3236 (1998).
[118] J. Seres, E. Seres, A. Verhoef *et al.*, *Nature* **433**, 596 (2005).
[119] M. C. Chen, P. Arpin, T. Popmintchev *et al.*, *Phys. Rev. Lett.* **105**, 173901 (2010).
[120] J. L. Krause, K. J. Schafer and K. C. Kulander, *Phys. Rev. Lett.* **68**, 3535 (1992).
[121] A. L'Huillier, M. Lewenstein, P. Salières *et al.*, *Phys. Rev. A* **48**, R3433 (1993).
[122] M. Lewenstein, P. Balcou, M. Y. Ivanov, A. L'Huillier and P. B. Corkum, *Phys. Rev. A* **49**, 2117 (1994).
[123] P. Agostini and L. F. DiMauro, *Rep. Prog. Phys.* **67**, 813 (2004).
[124] A. Scrinzi, M. Ivanov, R. Kienberger and D. Villeneuve, *J. Phys. B* **39**, R1 (2006).
[125] H. Niikura and P. B. Corkum, *Adv. At. Mol. Opt. Phys.* **54**, 511 (2007).
[126] F. Krausz and M. Ivanov, *Rev. Mod. Phys.* **81**, 163 (2009).
[127] T. W. Hänsch, *Opt. Commun.* **80**, 70 (1990).
[128] G. Farkas and C. Toth, *Phys. Lett. A* **168**, 447 (1992).
[129] S. E. Harris, J. J. Macklin and T. W. Hänsch, *Opt. Commun.* **100**, 487 (1993).
[130] O. Svelto, *Principles of Lasers*, 4th edn (New York: Plenum Press, 1998).
[131] P. Antoine, A. L'Huillier and M. Lewenstein, *Phys. Rev. Lett.* **77**, 1234 (1996).
[132] P. M. Paul, E. S. Toma, P. Breger *et al.*, *Science* **292**, 1689 (2001).
[133] P. B. Corkum, N. H. Burnett and M. Y. Ivanov, *Opt. Lett.* **19**, 1870 (1994).
[134] M. Ivanov, P. B. Corkum, T. Zuo and A. Bandrauk, *Phys. Rev. Lett* **74**, 2933 (1995).
[135] V. T. Platonenko and V. V. Strelkov, *J. Opt. Soc. Am. B* **16**, 435 (1999).
[136] K. S. Budil, P. Salières, A. L'Huillier, T. Ditmire and M. D. Perry, *Phys. Rev. A* **48**, R3437 (1993).
[137] C. Altucci, C. Delfin, L. Roos *et al.*, *Phys. Rev. A* **58**, 3934 (1998).
[138] M. Kovacev, Y. Mairesse, E. Priori *et al.*, *Eur. Phys. J. D* **26**, 79 (2003).
[139] O. Tcherbakoff, E. Mével, D. Descamps, J. Plumridge and E. Constant, *Phys. Rev. A* **68**, 043804 (2003).
[140] H. Mashiko, S. Gilbertson, C. Li *et al.*, *Phys. Rev. Lett.* **100**, 103906 (2008).
[141] I. P. Christov, M. M. Murnane and H. C. Kapteyn, *Phys. Rev. Lett.* **78**, 1251 (1997).
[142] M. Hentschel, R. Kienberger, C. Spielmann *et al.*, *Nature* **414**, 509 (2001).
[143] R. Kienberger, E. Gouliemakis, M. Uiberacker *et al.*, *Nature* **427**, 817 (2004).
[144] G. Sansone, E. Benedetti, F. Calegari *et al.*, *Science* **314**, 443 (2006).
[145] M. Casu, C. Szymanowski, S. Hu and C. H. Keitel, *J. Phys. B* **33**, L411 (2000).
[146] R. M. Potvliege, N. J. Kylstra and C. J. Joachain, *J. Phys. B* **33**, L743 (2000).
[147] D. M. Gaudiosi, B. Reagan, T. Popmintchev *et al.*, *Phys. Rev. Lett.* **96**, 203001 (2006).
[148] M. W. Walser, C. H. Keitel, A. Scrinzi and T. Brabec, *Phys. Rev. Lett.* **85**, 5082 (2000).
[149] N. J. Kylstra, R. M. Potvliege and C. J. Joachain, *J. Phys. B* **34**, L55 (2001).
[150] D. B. Milosevic, S. X. Hu and W. Becker, *Phys. Rev. A* **63**, R011403 (2001).
[151] N. J. Kylstra, R. M. Potvliege and C. J. Joachain, *Laser Phys.* **12**, 409 (2002).

[152] C. C. Chirilă, N. J. Kylstra, R. M. Potvliege and C. J. Joachain, *Phys. Rev. A* **66**, 063411 (2002).
[153] M. Gavrila, Free-free transitions of electron-atom systems in intense radiation fields. In F. A. Gianturco, ed., *Collision Theory for Atoms and Molecules* (New York: Plenum Press, 1989), p. 139.
[154] P. Francken and C. J. Joachain, *J. Opt. Soc. Am. B* **7**, 554 (1990).
[155] N. J. Mason, *Rep. Progr. Phys.* **56**, 1275 (1993).
[156] F. Ehlotzky, A. Jaron and J. Z. Kaminski, *Phys. Rep.* **297**, 63 (1998).
[157] A. Weingartshofer, J. K. Holmes, G. Caudle, E. M. Clarke and H. Kruger, *Phys. Rev. Lett.* **39**, 269 (1977).
[158] A. Weingartshofer, J. K. Holmes, J. Sabbagh and S. L. Chin, *J. Phys. B* **16**, 1805 (1983).
[159] B. Wallbank and J. K. Holmes, *J. Phys. B* **27**, 1221 (1994).
[160] N. J. Mason and W. R. Newell, *J. Phys. B* **20**, L323 (1987).
[161] S. Luan, R. Hippler and H. O. Lutz, *J. Phys. B* **24**, 3241 (1991).
[162] C. Höhr, A. Dorn, B. Najjari, D. Fischer, C. Schröter and J. Ullrich, *Phys. Rev. Lett.* **94**, 153201 (2005).
[163] N. J. Kylstra and C. J. Joachain, *Phys. Rev. A* **58**, R26 (1998).
[164] N. J. Kylstra and C. J. Joachain, *Phys. Rev. A* **60**, 2255 (1999).
[165] F. V. Bunkin and M. V. Fedorov, *Sov. Phys. JETP* **22**, 844 (1966).
[166] N. M. Kroll and K. M. Watson, *Phys. Rev. A* **8**, 804 (1973).
[167] C. J. Joachain, *Quantum Collision Theory*, 3rd edn (Amsterdam: North Holland, 1983).
[168] B. H. Bransden and C. J. Joachain, *Physics of Atoms and Molecules*, 2nd edn (Harlow, UK: Prentice Hall-Pearson, 2003).
[169] F. W. Byron and C. J. Joachain, *J. Phys. B* **17**, L295 (1984).

2

Theory of laser–atom interactions

In this chapter, we shall discuss the theory of laser–atom interactions, using a *semi-classical* method in which the laser field is treated classically, while the atom is studied by using quantum mechanics. This semi-classical approach constitutes an excellent approximation for intense laser fields, since in that case the number of photons per laser mode is very large [1, 2]. In addition, spontaneous emission can be neglected. We begin therefore by giving in Section 2.1 a classical description of the laser field in terms of electric- and magnetic-field vectors satisfying Maxwell's equations. We start by considering plane wave solutions of these equations. Then general solutions describing laser pulses are introduced. The dynamics of a classical electron in the laser field, and in particular the *ponderomotive energy* and *force*, are discussed in Section 2.2. Neglecting first relativistic effects, we write down in Section 2.3 the *time-dependent Schrödinger equation* (TDSE), which is the starting point of the theoretical study of atoms in intense laser fields, and introduce the *dipole approximation*. In the subsequent two sections, we study the behavior of the TDSE under *gauge transformations* and the *Kramers frame transformation*. In view of the central role that the time evolution operator plays in the development of the theory of laser–atom interactions, some general properties of this operator are reviewed in Section 2.6. In Section 2.7, the TDSE is solved explicitly for the simple case of a "free" electron in a laser field to obtain the *non-relativistic Gordon–Volkov wave functions*. In Section 2.8, we discuss the *non-relativistic, non-dipole* regime of laser–atom interactions. Finally, in Section 2.9, *relativistic effects* in laser–atom interactions are taken into account, and the appropriate relativistic wave equations are discussed.

2.1 Classical description of a laser field

The classical electromagnetic field generated by a laser is described in vacuo by electric and magnetic fields, $\boldsymbol{\mathcal{E}}(\mathbf{r}, t)$ and $\boldsymbol{\mathcal{B}}(\mathbf{r}, t)$, which satisfy Maxwell's equations

without sources:

$$\begin{aligned}\nabla\cdot\boldsymbol{\mathcal{E}}&=0,\\ \nabla\cdot\boldsymbol{\mathcal{B}}&=0,\\ \nabla\times\boldsymbol{\mathcal{E}}&=-\frac{\partial\boldsymbol{\mathcal{B}}}{\partial t},\\ \nabla\times\boldsymbol{\mathcal{B}}&=\frac{1}{c^2}\frac{\partial\boldsymbol{\mathcal{E}}}{\partial t},\end{aligned}\tag{2.1}$$

where c is the velocity of light in vacuo. The electric and magnetic fields can be generated from scalar and vector potentials, $\phi(\mathbf{r},t)$ and $\mathbf{A}(\mathbf{r},t)$, respectively, by the following relations:

$$\boldsymbol{\mathcal{E}}=-\nabla\phi-\frac{\partial\mathbf{A}}{\partial t}\tag{2.2}$$

and

$$\boldsymbol{\mathcal{B}}=\nabla\times\mathbf{A}.\tag{2.3}$$

In addition, from Equations (2.1)–(2.3) it follows that the vector potential $\mathbf{A}$ satisfies the homogeneous wave equation (as do ϕ, $\boldsymbol{\mathcal{E}}$ and $\boldsymbol{\mathcal{B}}$)

$$\nabla^2\mathbf{A}-\frac{1}{c^2}\frac{\partial^2\mathbf{A}}{\partial t^2}=0.\tag{2.4}$$

The potentials ϕ and $\mathbf{A}$ are not uniquely defined by these equations, since the fields $\boldsymbol{\mathcal{E}}$ and $\boldsymbol{\mathcal{B}}$ are invariant under the (classical) *gauge transformation*

$$\begin{aligned}\mathbf{A}&\rightarrow\mathbf{A}'=\mathbf{A}+\nabla f,\\ \phi&\rightarrow\phi'\ =\phi-\partial f/\partial t,\end{aligned}\tag{2.5}$$

where f is an arbitrary real, differentiable function of $\mathbf{r}$ and t. The freedom implied by the *gauge invariance* (2.5) means that one can choose a set of potentials $(\phi,\mathbf{A})$ which satisfy the *Lorentz condition*

$$\nabla\cdot\mathbf{A}+\frac{1}{c^2}\frac{\partial\phi}{\partial t}=0.\tag{2.6}$$

The potentials satisfying this condition are said to belong to the *Lorentz gauge*.

Another useful gauge for the potentials is the *Coulomb* (or radiation) *gauge*, which is defined by the condition

$$\nabla\cdot\mathbf{A}=0.\tag{2.7}$$

The Coulomb gauge is often used when no sources are present. Then $\phi=0$, and the fields are given by

$$\boldsymbol{\mathcal{E}}=-\frac{\partial\mathbf{A}}{\partial t}\tag{2.8}$$

and

$$\boldsymbol{\mathcal{B}} = \boldsymbol{\nabla} \times \mathbf{A}. \tag{2.9}$$

2.1.1 Plane wave solutions of Maxwell's equations

A monochromatic plane wave solution of Equation (2.4) corresponding to the angular frequency ω, i.e. to the frequency $\nu = \omega/(2\pi)$ and wavelength $\lambda = c/\nu$, is given by

$$\mathbf{A}(\mathbf{r}, t) = \hat{\boldsymbol{\epsilon}} A_0 \sin(\mathbf{k}_\mathrm{L} \cdot \mathbf{r} - \omega t - \varphi), \tag{2.10}$$

where $\mathbf{k}_\mathrm{L}$ is the *propagation vector* of the laser field, φ is a real constant phase and

$$\omega = k_\mathrm{L} c. \tag{2.11}$$

The Coulomb gauge condition (2.7) is satisfied if

$$\mathbf{k}_\mathrm{L} \cdot \hat{\boldsymbol{\epsilon}} = 0 \tag{2.12}$$

so that $\hat{\boldsymbol{\epsilon}}$ is perpendicular to $\mathbf{k}_\mathrm{L}$ and the wave is said to be *transverse*.

The corresponding electric field is given by

$$\boldsymbol{\mathcal{E}}(\mathbf{r}, t) = \hat{\boldsymbol{\epsilon}} \mathcal{E}_0 \cos(\mathbf{k}_\mathrm{L} \cdot \mathbf{r} - \omega t - \varphi), \tag{2.13}$$

with the electric-field strength given by $\mathcal{E}_0 = \omega A_0$. The quantity A_0, which we take to be positive, is the amplitude of the vector potential. Both the vector potential $\mathbf{A}$ and the electric field $\boldsymbol{\mathcal{E}}$ are in the direction of the real unit vector $\hat{\boldsymbol{\epsilon}}$, which is called the *polarization vector*. Using Equations (2.9) and (2.11), the magnetic field arising from the vector potential (2.10) is given by

$$\boldsymbol{\mathcal{B}}(\mathbf{r}, t) = \frac{\mathcal{E}_0}{c} (\hat{\mathbf{k}}_\mathrm{L} \times \hat{\boldsymbol{\epsilon}}) \cos(\mathbf{k}_\mathrm{L} \cdot \mathbf{r} - \omega t - \varphi). \tag{2.14}$$

From Equations (2.12)–(2.14) it follows that the vectors $\boldsymbol{\mathcal{E}}$, $\boldsymbol{\mathcal{B}}$ and $\mathbf{k}_\mathrm{L}$ are mutually orthogonal. Moreover, we see that

$$\frac{|\boldsymbol{\mathcal{B}}|}{|\boldsymbol{\mathcal{E}}|} = \frac{1}{c}. \tag{2.15}$$

An electromagnetic plane wave described by Equations (2.13) and (2.14), for which the electric-field vector points in a *fixed* (time-independent) direction $\hat{\boldsymbol{\epsilon}}$, is said to be *linearly polarized*. A *general state of polarization* for a plane wave propagating in the direction $\hat{\mathbf{k}}_\mathrm{L}$ can be described by combining two independent linearly polarized plane waves with real unit polarization vectors $\hat{\boldsymbol{\epsilon}}_a$ and $\hat{\boldsymbol{\epsilon}}_b$ perpendicular

to $\mathbf{k}_{\mathrm{L}}$, where the phases of the two component waves are, in general, different. The corresponding vector potential and electric field are given by

$$\mathbf{A}(\mathbf{r},t) = \hat{\boldsymbol{\epsilon}}_a A_{0,a} \sin(\mathbf{k}_{\mathrm{L}} \cdot \mathbf{r} - \omega t - \varphi_a) + \hat{\boldsymbol{\epsilon}}_b A_{0,b} \sin(\mathbf{k}_{\mathrm{L}} \cdot \mathbf{r} - \omega t - \varphi_b) \tag{2.16}$$

and

$$\boldsymbol{\mathcal{E}}(\mathbf{r},t) = \hat{\boldsymbol{\epsilon}}_a \mathcal{E}_{0,a} \cos(\mathbf{k}_{\mathrm{L}} \cdot \mathbf{r} - \omega t - \varphi_a) + \hat{\boldsymbol{\epsilon}}_b \mathcal{E}_{0,b} \cos(\mathbf{k}_{\mathrm{L}} \cdot \mathbf{r} - \omega t - \varphi_b), \tag{2.17}$$

where $A_{0,a}$ and $A_{0,b}$ are positive quantities, $\mathcal{E}_{0,a} = \omega A_{0,a}$ and $\mathcal{E}_{0,b} = \omega A_{0,a}$. It is always possible to find a phase φ, a real number ξ such that $-1 \leq \xi \leq 1$, and two unit vectors $\hat{\boldsymbol{\epsilon}}_1$ and $\hat{\boldsymbol{\epsilon}}_2$ forming with $\hat{\mathbf{k}}_{\mathrm{L}}$ a right-handed orthogonal coordinate system, so that the vector potential (2.16) can also be written in the form

$$\mathbf{A}(\mathbf{r},t) = \frac{A_0}{(1+\xi^2)^{1/2}} \left[\hat{\boldsymbol{\epsilon}}_1 \sin(\mathbf{k}_{\mathrm{L}} \cdot \mathbf{r} - \omega t - \varphi) - \xi \hat{\boldsymbol{\epsilon}}_2 \cos(\mathbf{k}_{\mathrm{L}} \cdot \mathbf{r} - \omega t - \varphi)\right]. \tag{2.18}$$

The electric field corresponding to the vector potential (2.18) can be expressed as

$$\boldsymbol{\mathcal{E}}(\mathbf{r},t) = \frac{\mathcal{E}_0}{(1+\xi^2)^{1/2}} \left[\hat{\boldsymbol{\epsilon}}_1 \cos(\mathbf{k}_{\mathrm{L}} \cdot \mathbf{r} - \omega t - \varphi) + \xi \hat{\boldsymbol{\epsilon}}_2 \sin(\mathbf{k}_{\mathrm{L}} \cdot \mathbf{r} - \omega t - \varphi)\right], \tag{2.19}$$

with $\mathcal{E}_0 = \omega A_0$.

The constant ξ is the *ellipticity parameter* of the radiation field, which, upon varying in the range $-1 \leq \xi \leq 1$, describes all possible cases of polarization. The value $\xi = 0$ corresponds to linear polarization. For $\xi = \pm 1$, the monochromatic plane wave is said to be *circularly polarized*. At a fixed point in space, the electric-field vector $\boldsymbol{\mathcal{E}}$ is constant in magnitude and, as a function of time, traces out a circle at an angular frequency ω in the plane of the vectors $\hat{\boldsymbol{\epsilon}}_1$ and $\hat{\boldsymbol{\epsilon}}_2$ perpendicular to the propagation vector $\mathbf{k}_{\mathrm{L}}$. As a function of $\mathbf{r}$, for a fixed time, the vector $\boldsymbol{\mathcal{E}}$ traces a helix. If $\xi = -1$, the rotation of $\boldsymbol{\mathcal{E}}$ as a function of time at a fixed point is counter-clockwise for an observer facing into the oncoming wave (looking into the direction $-\hat{\mathbf{k}}_{\mathrm{L}}$), while at a fixed time the helix is left-handed. This wave is said to be *left-circularly polarized*.

Such a wave is also said to have *positive helicity* because it has a positive projection of angular momentum on the propagation direction $\hat{\mathbf{k}}_{\mathrm{L}}$. If $\xi = 1$, the rotation of the vector $\boldsymbol{\mathcal{E}}$ as a function of time at a fixed point in space is clockwise for an observer facing into the incoming wave and the helix is right-handed. This wave is said to be *right-circularly polarized*; it is said to have *negative helicity*, because it has a negative projection of angular momentum on the propagation direction $\hat{\mathbf{k}}_{\mathrm{L}}$. When $0 < |\xi| < 1$, the vector $\boldsymbol{\mathcal{E}}$, at a fixed point of space, traces out an ellipse as a function of time in the plane of the vectors $\hat{\boldsymbol{\epsilon}}_1$ and $\hat{\boldsymbol{\epsilon}}_2$. Such a wave is said to be *elliptically polarized*.

In order to explore in more detail the concept of polarization, we write the electric-field vector (2.19) corresponding to a monochromatic plane wave of arbitrary polarization in the following form:

$$\boldsymbol{\mathcal{E}}(\mathbf{r},t) = \mathcal{E}_0 \mathrm{Re}\left\{\hat{\boldsymbol{\epsilon}}_\mathrm{c} \exp\left[\mathrm{i}(\mathbf{k}_\mathrm{L}\cdot\mathbf{r} - \omega t - \varphi)\right]\right\}. \tag{2.20}$$

In the above equation, $\hat{\boldsymbol{\epsilon}}_\mathrm{c}$ is a *complex* unit polarization vector such that

$$\hat{\boldsymbol{\epsilon}}_\mathrm{c}^* \cdot \hat{\boldsymbol{\epsilon}}_\mathrm{c} = 1. \tag{2.21}$$

This vector can be written as a linear combination of the two basis vectors $\hat{\boldsymbol{\epsilon}}_1$ and $\hat{\boldsymbol{\epsilon}}_2$, namely

$$\hat{\boldsymbol{\epsilon}}_\mathrm{c} = c_1\hat{\boldsymbol{\epsilon}}_1 + c_2\hat{\boldsymbol{\epsilon}}_2, \tag{2.22}$$

where the complex coefficients c_1 and c_2 satisfy the equation

$$|c_1|^2 + |c_2|^2 = 1. \tag{2.23}$$

We note that Equation (2.20) reduces to Equation (2.19) if we take

$$c_1 = \frac{1}{(1+\xi^2)^{1/2}}, \qquad c_2 = \frac{-\mathrm{i}\xi}{(1+\xi^2)^{1/2}}. \tag{2.24}$$

Let us write the two complex coefficients c_1 and c_2 in the form

$$c_1 = |c_1|\exp(\mathrm{i}\alpha), \qquad c_2 = |c_2|\exp(\mathrm{i}\beta). \tag{2.25}$$

If the phases α and β are equal (modulo π), so that $\alpha = \beta + m\pi$ (with $m = 0, \pm1, \pm2, \ldots$), the electric-field vector (2.20) can be written in the form

$$\begin{aligned}\boldsymbol{\mathcal{E}}(\mathbf{r},t) &= \mathcal{E}_0 \mathrm{Re}\left\{(|c_1|\hat{\boldsymbol{\epsilon}}_1 \pm |c_2|\hat{\boldsymbol{\epsilon}}_2)\exp\left[\mathrm{i}(\mathbf{k}_\mathrm{L}\cdot\mathbf{r} - \omega t - \varphi + \alpha)\right]\right\} \\ &= \mathcal{E}_0(|c_1|\hat{\boldsymbol{\epsilon}}_1 \pm |c_2|\hat{\boldsymbol{\epsilon}}_2)\cos\left(\mathbf{k}_\mathrm{L}\cdot\mathbf{r} - \omega t - \varphi + \alpha\right),\end{aligned} \tag{2.26}$$

and we see that the direction of the vector $\boldsymbol{\mathcal{E}}$ is independent of time, so that the monochromatic plane wave (2.26) is linearly polarized. If the amplitudes of the coefficients c_i are equal, so that $|c_1| = |c_2| = 1/\sqrt{2}$, but the phases α and β differ by $\pi/2$ (modulo 2π), i.e. $\beta = \alpha \pm \pi/2 + 2m\pi$ (with $m = 0, \pm1, \pm2, \ldots$), then the electric field can be written as

$$\begin{aligned}\boldsymbol{\mathcal{E}}(\mathbf{r},t) &= \frac{\mathcal{E}_0}{\sqrt{2}}\mathrm{Re}\left\{(\hat{\boldsymbol{\epsilon}}_1 \pm \mathrm{i}\hat{\boldsymbol{\epsilon}}_2)\exp\left[\mathrm{i}(\mathbf{k}_\mathrm{L}\cdot\mathbf{r} - \omega t - \varphi + \alpha)\right]\right\} \\ &= \frac{\mathcal{E}_0}{\sqrt{2}}\left\{\hat{\boldsymbol{\epsilon}}_1\cos\left(\mathbf{k}_\mathrm{L}\cdot\mathbf{r} - \omega t - \varphi + \alpha\right) \mp \hat{\boldsymbol{\epsilon}}_2\sin\left(\mathbf{k}_\mathrm{L}\cdot\mathbf{r} - \omega t - \varphi + \alpha\right)\right\},\end{aligned} \tag{2.27}$$

and the monochromatic plane wave (2.27) is left-circularly polarized if the upper sign is selected and right-circularly polarized if the lower sign is selected. If the complex coefficients c_1 and c_2 in Equation (2.22) do not correspond to either linear or circular polarization, the wave is elliptically polarized.

In the above discussion, we have described a general state of polarization for a monochromatic plane wave by using two linearly polarized waves to form a set of basis fields, with real, orthogonal unit polarization vectors $\hat{\boldsymbol{\epsilon}}_1$ and $\hat{\boldsymbol{\epsilon}}_2$ in a plane perpendicular to $\hat{\mathbf{k}}_\mathrm{L}$. The complex polarization vector $\hat{\boldsymbol{\epsilon}}_\mathrm{c}$ was then expanded in terms of these basis vectors. The two circularly polarized waves (2.27) constitute an equally acceptable set of basic fields for the description of an arbitrary state of polarization. We introduce the two complex orthogonal unit basis vectors

$$\hat{\boldsymbol{\epsilon}}_\mathrm{l} = \frac{1}{\sqrt{2}}\left(\hat{\boldsymbol{\epsilon}}_1 + \mathrm{i}\hat{\boldsymbol{\epsilon}}_2\right), \qquad \hat{\boldsymbol{\epsilon}}_\mathrm{r} = \frac{1}{\sqrt{2}}\left(\hat{\boldsymbol{\epsilon}}_1 - \mathrm{i}\hat{\boldsymbol{\epsilon}}_2\right), \tag{2.28}$$

which correspond to left- and right-circular polarization, respectively. These vectors are such that

$$\hat{\boldsymbol{\epsilon}}_\mathrm{l}^* \cdot \hat{\boldsymbol{\epsilon}}_\mathrm{l} = \hat{\boldsymbol{\epsilon}}_\mathrm{r}^* \cdot \hat{\boldsymbol{\epsilon}}_\mathrm{r} = 1 \tag{2.29}$$

and

$$\hat{\boldsymbol{\epsilon}}_\mathrm{l}^* \cdot \hat{\boldsymbol{\epsilon}}_\mathrm{r} = \hat{\boldsymbol{\epsilon}}_\mathrm{r}^* \cdot \hat{\boldsymbol{\epsilon}}_\mathrm{l} = \hat{\boldsymbol{\epsilon}}_\mathrm{l}^* \cdot \hat{\mathbf{k}}_\mathrm{L} = \hat{\boldsymbol{\epsilon}}_\mathrm{r}^* \cdot \hat{\mathbf{k}}_\mathrm{L} = 0. \tag{2.30}$$

A general state of polarization can then be specified by a complex unit polarization vector $\hat{\boldsymbol{\epsilon}}_\mathrm{c}$ such that

$$\hat{\boldsymbol{\epsilon}}_\mathrm{c} = c_\mathrm{l}\,\hat{\boldsymbol{\epsilon}}_\mathrm{l} + c_\mathrm{r}\,\hat{\boldsymbol{\epsilon}}_\mathrm{r}, \tag{2.31}$$

where c_l and c_r are complex coefficients satisfying the equation

$$|c_\mathrm{l}|^2 + |c_\mathrm{r}|^2 = 1. \tag{2.32}$$

Throughout this book, we will assume that the polarization of the laser field is known, so that partially polarized fields will not be considered.

The energy density of the monochromatic electromagnetic field is given by

$$\frac{1}{2}(\epsilon_0|\boldsymbol{\mathcal{E}}|^2 + \mu_0^{-1}|\boldsymbol{\mathcal{B}}|^2) = \frac{\epsilon_0\mathcal{E}_0^2}{1+\xi^2}\left[\cos^2(\mathbf{k}_\mathrm{L}\cdot\mathbf{r} - \omega t - \varphi) + \xi^2\sin^2(\mathbf{k}_\mathrm{L}\cdot\mathbf{r} - \omega t - \varphi)\right], \tag{2.33}$$

where ϵ_0 and μ_0 are the permittivity and permeability of free space, respectively, and $\epsilon_0\mu_0 = c^{-2}$. Averaging the energy density over a period $T = 2\pi/\omega$, and using the fact that

$$\frac{1}{T}\int_0^T \sin^2(\mathbf{k}_\mathrm{L}\cdot\mathbf{r} - \omega t - \varphi)\mathrm{d}t = \frac{1}{T}\int_0^T \cos^2(\mathbf{k}_\mathrm{L}\cdot\mathbf{r} - \omega t - \varphi)\mathrm{d}t = \frac{1}{2}, \tag{2.34}$$

the cycle-averaged energy density at the given angular frequency ω is found to be

$$\rho(\omega) = \frac{1}{2}\epsilon_0 \mathcal{E}_0^2 = \frac{1}{2}\epsilon_0 \omega^2 A_0^2 . \tag{2.35}$$

It is interesting to relate this result to the photon density, keeping in mind that each photon at a frequency ν carries a quantum of energy $h\nu = \hbar\omega$. If $\mathcal{N}(\omega)$ denotes the number of photons of angular frequency ω within a volume V, the energy density is given by

$$\rho(\omega) = \frac{\hbar\omega \mathcal{N}(\omega)}{V} . \tag{2.36}$$

From Equations (2.35) and (2.36), we find that

$$\mathcal{E}_0^2 = \frac{2\rho(\omega)}{\epsilon_0} = \frac{2\hbar\omega \mathcal{N}(\omega)}{\epsilon_0 V} . \tag{2.37}$$

The Poynting vector

$$\boldsymbol{\mathcal{S}} = \frac{1}{\mu_0}(\boldsymbol{\mathcal{E}} \times \boldsymbol{\mathcal{B}}) \tag{2.38}$$

is in the direction of the propagation vector $\mathbf{k}_\mathrm{L}$. Its magnitude is the rate of energy flow through a unit area normal to the direction of propagation. Averaged over a period, T, this quantity gives the intensity $I(\omega)$ associated with the monochromatic plane wave (2.19) of angular frequency ω. That is,

$$I(\omega) = \frac{1}{2}\epsilon_0 c \mathcal{E}_0^2 = \frac{1}{2}\epsilon_0 c \omega^2 A_0^2 . \tag{2.39}$$

It should be noted that the definition of the electric-field strength introduced in Equation (2.19) implies that the intensity (2.39) does not depend on the ellipticity parameter ξ. From Equations (2.36), (2.37) and (2.39) we also have

$$I(\omega) = \rho(\omega) c = \frac{\hbar\omega \mathcal{N}(\omega) c}{V} . \tag{2.40}$$

Finally, the photon flux of the field is given by

$$\Phi(\omega) = \frac{I(\omega)}{\hbar\omega} . \tag{2.41}$$

As an example, let us consider a linearly polarized laser field generated by a Nd:YAG laser with photon energy $\hbar\omega = 1.17\,\mathrm{eV}$. Even for a modest intensity $I = 10^{12}\,\mathrm{W\,cm^{-2}}$, the number of photons in a coherence volume $V = \lambda^3$ (with $\lambda = 2\pi c/\omega = 1064\,\mathrm{nm}$), as obtained from Equation (2.40), is

$$\mathcal{N} = \frac{IV}{\hbar\omega c} \simeq 2 \times 10^8 , \tag{2.42}$$

which is very large. A classical description of the laser field is therefore justified. We point out that a more rigorous justification of this statement can be given by using the fact that, to a good approximation, the radiation generated by a laser is in a coherent state, which is the quantum electrodynamic state approximating most closely the classical state of the field [3–5]. For large values of the average number of photons in the coherent state, quantum corrections only cause small fluctuations about the classical field.

2.1.2 Laser pulses

Thus far, we have considered only monochromatic plane wave solutions of Equation (2.4). As we will see later, the electromagnetic field can often be taken to be monochromatic when describing the interaction of an atom with a "long" laser pulse, lasting tens of optical cycles or more. However, this is not the case for shorter laser pulses, in particular for ultra-short pulses lasting a few optical cycles or even less. In what follows, we shall give a brief theoretical description of laser pulses.

A general laser pulse can be formed by superimposing monochromatic plane waves with appropriate amplitudes, frequencies and phases. It is useful to distinguish between pulses that are *spatially homogeneous* in the plane perpendicular to the laser propagation vector $\mathbf{k}_{\mathrm{L}}$ and *focused* laser pulses. We begin by discussing the former. We shall consider the simple case where each plane wave component has the same direction of propagation $\hat{\mathbf{k}}_{\mathrm{L}}$ and is linearly polarized in the direction $\hat{\boldsymbol{\epsilon}}$. The vector potential in the Coulomb gauge can then be written as

$$\mathbf{A}(\mathbf{r},t) = \hat{\boldsymbol{\epsilon}} \int_0^\infty A_0(\omega') \sin[\mathbf{k}'_{\mathrm{L}} \cdot \mathbf{r} - \omega' t - \varphi(\omega')]\, \mathrm{d}\omega', \tag{2.43}$$

where $\varphi(\omega')$ is the phase associated with the angular frequency ω' and $\mathbf{k}'_{\mathrm{L}} = (\omega'/c)\hat{\mathbf{k}}_{\mathrm{L}}$. Since the laser pulse is localized in space and time, the amplitude $A_0(\omega')$ is peaked about the pulse *carrier angular frequency* ω, while its "width" is inversely proportional to the pulse duration. If the laser field is monochromatic, then $A_0(\omega')$ reduces to $A_0\delta(\omega' - \omega)$, where $\delta(x)$ denotes the Dirac delta function. Both $\varphi(\omega')$ and $A_0(\omega')$ are in general smooth functions. However, for ultra-short pulses $A_0(\omega')$ may vary in a complicated way and extend over a wide range of frequencies.

Using the plane wave expansion (2.43) for the vector potential, the electric-field component of the laser pulse is found to be

$$\boldsymbol{\mathcal{E}}(\mathbf{r},t) = \hat{\boldsymbol{\epsilon}} \int_0^\infty \mathcal{E}_0(\omega') \cos[\mathbf{k}'_{\mathrm{L}} \cdot \mathbf{r} - \omega' t - \varphi(\omega')]\, \mathrm{d}\omega', \tag{2.44}$$

where the quantity $\mathcal{E}_0(\omega') = \omega' A(\omega')$ has the dimensions of an electric-field amplitude per unit angular frequency.

The total energy flux passing through a plane of unit area perpendicular to the propagation vector $\mathbf{k}_\mathrm{L}$ must be finite. Using Equation (2.38), together with Equations (2.44) and (2.15), we have

$$\int_{-\infty}^{\infty} \hat{\mathbf{k}}_\mathrm{L} \cdot \boldsymbol{\mathcal{S}}(t)\,\mathrm{d}t = \pi\epsilon_0 c \int_0^{\infty} \mathcal{E}_0^2(\omega')\mathrm{d}\omega' \;<\; \infty \tag{2.45}$$

so that $\mathcal{E}_0^2(\omega')$ must decrease faster than $(\omega')^{-1}$ as ω' goes to infinity. In addition, due to the finite size of the laser oscillator, the laser pulse cannot contain angular frequencies that are smaller than some minimum cut-off angular frequency $\omega_\mathrm{min} > 0$. Therefore

$$\mathcal{E}_0(\omega') = 0, \quad \omega' < \omega_\mathrm{min}. \tag{2.46}$$

The existence of this cut-off allows one to deduce two properties of a laser pulse that is described by the vector potential (2.43). Let us consider the following integral over the electric-field component of the laser pulse:

$$\begin{aligned}\lim_{t\to\infty} \int_{-t}^{t} \boldsymbol{\mathcal{E}}(\mathbf{r},t')\mathrm{d}t' &= \lim_{t\to\infty} [\mathbf{A}(\mathbf{r},-t) - \mathbf{A}(\mathbf{r},t)] \\ &= \lim_{t\to\infty} 2\hat{\boldsymbol{\epsilon}} \int_0^{\infty} \frac{\mathcal{E}_0(\omega')}{\omega'} \sin(\omega' t)\cos[\mathbf{k}'_\mathrm{L}\cdot\mathbf{r} - \varphi(\omega')]\mathrm{d}\omega'.\end{aligned} \tag{2.47}$$

Treating t as a parameter, we first calculate this limit by making use of the following representation of the Dirac delta function:

$$\delta(x) = \lim_{\epsilon\to 0^+} \frac{\sin(x/\epsilon)}{\pi x}. \tag{2.48}$$

Then, using Equation (2.46), it follows that

$$\lim_{t\to\infty} \int_{-t}^{t} \boldsymbol{\mathcal{E}}(\mathbf{r},t')\mathrm{d}t' = 0. \tag{2.49}$$

A similar calculation shows that

$$\lim_{t\to\infty} \int_{-t}^{t} \mathbf{A}(\mathbf{r},t')\mathrm{d}t' = 0. \tag{2.50}$$

We will see in Section 2.2 that the two results in Equations (2.49) and (2.50) have important implications for the dynamics of free electrons in laser fields.

In studying the interaction of laser pulses with atoms, the spatial profile of the laser pulse can be assumed to remain constant over atomic dimensions. In this